Nanoscale

REVIEW

View Article Online
View Journal | View Issue

Cite this: *Nanoscale*, 2025, **17**, 6390

Latest developments in the synthesis of metal–organic frameworks and their hybrids for hydrogen storage†

Laura Jimenez-Lopez, [a] Rafael Morales Ospino, [a] Leandro Goulart de Araujo, [a] Alain Celzard [a,b] and Vanessa Fierro *[a]

Metal–organic frameworks (MOFs) are promising materials for hydrogen (H_2) storage due to their versatile structures, high surface areas and substantial pore volumes. This paper provides a comprehensive review of MOF synthesis and characterization, as well as their practical applications for H_2 storage. We explore various MOF synthesis techniques, highlighting their impact on the nanopore structure and functionality. Special emphasis is placed on strategies for enhancing H_2 storage capacities by increasing specific surface areas, optimizing pore size distributions, and facilitating H_2 release by improving thermal conductivity. Key advances in MOF-based hybrids, such as MOFs combined with carbonaceous materials, metals or other inorganic materials, are discussed. This review also addresses the effectiveness of linker functionalization and the introduction of unsaturated metal centers to optimize H_2 storage under ambient conditions. We conclude that the development of competitive MOF-based hybrids, particularly those that incorporate carbons, offers significant potential for improving H_2 storage and recovery, enhancing thermal stability and increasing thermal conductivity. These advancements are in line with the US Department of Energy (DOE) specifications and pave the way for future research into the optimization of MOFs for practical H_2 storage applications.

Received 27th September 2024,
Accepted 1st February 2025

DOI: 10.1039/d4nr03969f

rsc.li/nanoscale

1. Introduction

Hydrogen (H_2) is a promising alternative energy carrier due to its potential to reduce greenhouse gas emissions when produced from renewable energy sources. However, efficient and safe storage of H_2 remains a major challenge.[1] Although H_2 has the highest specific energy density, 33.6 kW h kg^{-1}, it also has the lowest volumetric energy density, 0.0108 MJ L^{-1}, measured under standard conditions,[2] which is 3000 times less than that of gasoline.[3] Hydrogen appears to be one of the most promising alternatives to achieve carbon neutrality, offering a clean energy source to replace fossil fuels in industries, transportation and power systems.[4] Produced from renewables, it enables deep decarbonization and ensures a stable energy supply, driving the transition to a sustainable, low-carbon future.[5]

Storing H_2 at pressures above 70 MPa or at temperatures below −253 °C is a possible alternative for increasing H_2 density during transport and storage, but it requires harsh conditions and raises public safety concerns. Adsorption of H_2 at −196 °C, the boiling point of liquid nitrogen, enables H_2 to be stored at moderate pressures, of the order of 5 MPa, but requires high-surface area materials with a suitable pore size distribution (PSD) and high bulk density.

A wide range of carbon-based materials has been thoroughly studied for H_2 storage, showing that excess H_2 adsorption capacities at room temperature are lower, typically less than 2 wt%, compared with capacities observed at −196 °C, which remain generally below 7 wt%.[6] For this reason, metal–organic frameworks (MOFs) have emerged as promising candidates for H_2 storage due to their tunable porosity, high surface area and the possibility of tailoring their properties to specific applications.[7] Excess H_2 storage capacities in the range of 2.4 to 9.1 wt% have been obtained in MOFs with Brunauer–Emmett–Teller (BET) areas (A_{BET}) of up to 6000 m^2 g^{-1}. The highest H_2 storage capacity reported to date is 9.05 wt% at −196 °C and 7 MPa for NU100.[8]

Due to the limitations of the BET method, these very high A_{BET} values are more indicative of pore volume than the actual surface area. Indeed, when excess H_2 storage capacities at −196 °C are plotted as a function of A_{BET} for a large number of MOFs, the observed trend does not follow Chahine's heuristic

[a]*Université de Lorraine, CNRS, IJL, F-88000 Epinal, France.*
E-mail: vanessa.fierro@univ-lorraine.fr
[b]*Institut Universitaire de France (IUF), F-75231 Paris, France*

† Electronic supplementary information (ESI) available. See DOI: https://doi.org/10.1039/d4nr03969f

rule of 1 wt% H_2 per 500 m^2 g^{-1} of surface area. Moreover, increasing A_{BET} leads to an increase in average pore volume and thus to a decrease in adsorbent–sorbate interactions and isosteric enthalpy of adsorption. The increase in pore volume also results in a reduction of particle density. Indeed, while absolute gravimetric H_2 capacities reach values as high as 120 mg H_2 per g (12 wt%), volumetric H_2 capacities peak at values of around 40 kg H_2 per m^3. Thus, MOFs with high A_{BET} and high absolute H_2 uptake on a gravimetric basis are not necessarily those with the highest H_2 uptake on a volumetric basis.

In this field, MOF hybrids, *i.e.*, MOFs combined with other materials, such as other MOFs, carbon-based materials or metallic particles, have shown promise as a viable choice for H_2 adsorption by increasing their adsorption capacity through an increased specific surface area.[9,10] The addition of carbon-based materials to produce MOF hybrids can improve thermal conductivity and allow tuning of the chemical composition to provide greater selectivity[11] for H_2 adsorption compared with other gases. A bibliometric analysis (conducted in English in the Scopus database, followed by an analysis using the Bibliometrix package in R language) was carried out to give an overview of the use of MOFs for H_2 adsorption. A clear upward trend in the use of MOFs for H_2 storage is observed over time, with a peak of 111 publications in 2024 (last access 15 August 2024) (Fig. S1†). Another bibliometric analysis has been performed, now considering the use of MOF-based hybrids for H_2 adsorption. A clear upward trend in the use of MOF-based hybrid materials for H_2 storage is observed over time, especially after 2016, peaking in 2024 (last access 15 August 2024) with 27 publications, followed by 2019 and 2022 with 24 publications each (Fig. S2†).

This review aims to provide a comprehensive overview of the current state of research in H_2 storage, using MOFs as materials of interest, focusing on the enhancement of the properties of MOF hybrids, the challenges faced and future prospects, including their potential applications in the energy industry.

2. Basic aspects of MOF synthesis and characterization

MOFs or porous coordination polymers (PCPs) are materials containing metal ions connected by organic linkers to form a 3D network.[14] The metal ions form primary building units (PBUs) with precise geometric structures, linked by secondary building units (SBUs).[15] Commonly used metal ions include Cr^{3+}, Fe^{3+}, Co^{2+} and Zn^{2+},[16] with coordination numbers from 2 to 7, yielding various geometries such as linear, T-shaped, tetrahedral, square planar, octahedral, *etc.*[17] Organic linkers, such as carboxylates, phosphates, sulfonates, *etc.*, can form coordination bonds, with fumaric, succinic, and terephthalic acids being low-cost options. Other ligands such as peptides, carbohydrates, amino acids and cyclodextrins are also used.[18] Different classes of MOFs exist, of which "MOFs" is the abbreviation and general name,[19] and their discovery is the result of the collective efforts of many research groups and laboratories around the world. Several major laboratories have made significant contributions to the field of MOFs, including materials from Universitetet i Oslo (UIO), Institut Lavoiser (MIL) and Northwestern University (NU), among others (Fig. S3a†).

MOFs have high surface area, tunable pore size and diverse functionalities, making them attractive for various applications such as gas storage, separation, catalysis and sensing.[20] In Fig. 1a, $(-CO_2)x$ represents the organic linker, with x being the number of linkers associated with the cluster, giving rise to the crystalline geometry of the MOF. MOFs are also highly customizable, with the ability to vary not only the metal ion (Fig. 1b) and the organic linker (Fig. 1c), but also the synthesis conditions to tailor the material's properties and provide different varieties of MOFs with varied characteristics of interest.

2.1. MOF synthesis

The energy required for MOF synthesis, to allow linkage between PBUs and SBUs, can be provided by a variety of synthesis approaches, including solvothermal/hydrothermal, sonochemical, electrochemical, microwave-assisted and mechanochemical, which can be applied to produce MOFs with contrasting structures and features. Table 1 shows some advantages and disadvantages of each of these approaches, which are briefly reviewed, from the classical solvothermal/hydrothermal route to the Resonant Acoustic Mixing (RAM) route:

- **Solvothermal** (with organic solvents) **or hydrothermal synthesis** (with water) takes place in sealed vessels above the boiling point of the liquid medium under standard pressure.[21] Conventional solvothermal/hydrothermal synthesis involves heating metal ions, linkers and solvents together (80–200 °C)[22] in a polytetrafluoroethylene (PTFE)-lined autoclave (for high temperatures) or in scintillation vials (for lower temperatures).[16] The synergy of pressure, temperature and solvent produces single crystals due to the material's solubility in a hot and pressurized solvent, whether organic or aqueous,[22] which favors reaction and crystal growth. Although solvothermal/hydrothermal synthesis produces well-formed MOFs with controlled size, it requires longer synthesis times and often organic solvents. Zheng *et al.*[23] compared hydrothermal, reflux, vessel, and microwave methods to synthesize MOF-303 for water harvesting from desert air. The hydrothermal method took 24 h, while the reflux and vessel methods needed 4 to 8 h. Microwave synthesis was the fastest at 5 min.

- **Non-solvothermal synthesis** takes place at temperatures below the boiling point of the solvent under standard pressure, usually at room temperature.[16] For instance, some widely used MOFs such as MOF-5, MOF-74, MOF-177, HKUST-1, IRMOF-0, MIL-53(Al), MOF-2 and ZIF-7 have been successfully synthesized under ambient conditions.[24–28] The shape of the crystals obtained and the percentage of purity are strongly influenced by the reaction temperature.[29] Yields are also affected by

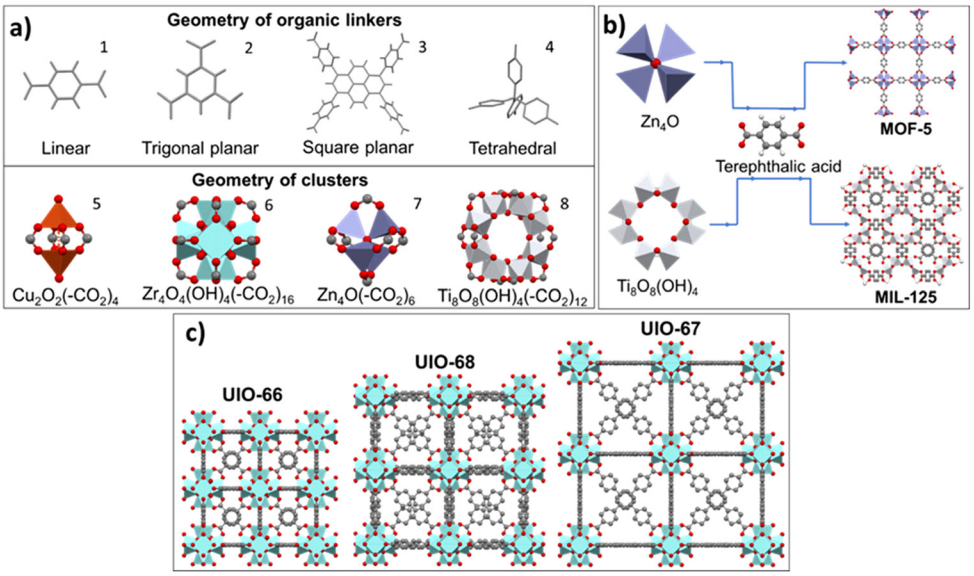

Fig. 1 (a) Geometry of some organic linkers (1: BDC; 2: BTC; 3: H4TBAPy and 4: tetraphenylmethane) (adapted from ref. 12 and 13), and geometry of some clusters; (b) assembly of two different clusters with the same organic linker to obtain two MOFs; (c) assembly of the same cluster ($Zr_4O_4(OH)_4(-CO_2)_{16}$) with 3 linkers to obtain three different MOFs.

temperature, as shown by Lestari *et al.*,[30] who reported a 24% yield for HKUST-1 at room temperature *versus* 99% at 120 °C. However, by using ambient temperature, other synthetic routes emerge as alternatives, broadening the horizons for future research.

- **Sonochemical synthesis** uses ultrasound to create nanomaterials with the help of sound-wave-induced bubbles. The small bubbles promote interactions between particles up to 13 eV, leading to significant reactions. The bubble stages – formation, growth and collapse – induce chemical reactions in the synthesis of MOFs.[31,32] Reaction time has a significant influence on crystal size in sonochemical synthesis. Qiu *et al.*[33] found that short runs (5–10 min) produced spherical nanocrystals of 50–100 nm, while longer runs (30–90 min) produced needle-shaped crystals of 700–900 nm. Vaitsis *et al.* concluded that ultrasound outperforms electrical and microwave heating due to its simplicity, faster reactions and improved energy efficiency, but with the use of organic solvents.[34]

- **Electrochemical synthesis** was first used to synthesize HKUST-1 in 2005, paving the way for various electrochemical methods and materials design for MOFs, including MOF-5,[35] MIL-53,[36] MIL-100(Fe)[37] and ZIF-8.[38] Electrosynthesis is practical and cost-effective, as it operates under milder conditions and within shorter timescales. It offers advantages such as mild reactions, easy operation and efficient charge transfer, which promotes rapid MOF crystal growth.[35,39] Antonio *et al.*[40] used electrosynthesis to prepare titanium(III)-based MOFs, namely Ti^{III}-MIL-101 and Ti^{III}-MIL-102, and extended it to other Ti^{III}-MIL structures using $TiCl_4$. The materials produced by electrosynthesis showed similar characteristics to the more expensive $TiCl_3$, demonstrating its cost-effectiveness. However, electrochemical synthesis often involves organic solvents, which can potentially impact the surface area, pore volume and thermal stability.[41]

- **Microwave-assisted synthesis** is an effective method for high-throughput syntheses, as it heats the material uniformly due to molecular dipolarity and ionic conduction.[42] Rapid microwave heating can generate hot spots that give rise to metastable materials.[43] However, after careful control of the synthesis conditions, this approach increases efficiency as crystals disperse throughout the solution, leading to faster and higher yields due to rapid consumption of reagents.[44] Although crystals are smaller than with traditional methods, microwave crystallization reduces synthesis time and material use while maintaining the surface area.[45–47] Wu *et al.*[48] synthesized conductive, partially carbonized metal–organic frameworks with ruthenium nanoparticles using household microwave ovens. Among them, Ru@p-Co3HHTP2-3.2% exhibited excellent performance in the electrocatalytic H_2 evolution reaction. These studies highlight the potential of microwave-assisted methods for the efficient synthesis of advanced materials with enhanced H_2-related properties, but they are generally associated with the use of organic solvents.

- **Ionothermal synthesis** uses ionic liquids (ILs) as solvents or templates, resulting in MOFs with a negatively charged skeleton structure. The IL cations are firmly integrated into the MOF framework.[49] ILs have properties that can be advantageous over traditional solvents, such as their extremely low vapor pressures. They can advantageously replace organic solvents such as *N*,*N*-dimethylformamide (DMF).[50] This synthesis can operate at lower temperatures such as 30 °C, consuming less energy than the solvothermal approach. Peng *et al.* synthesized mesoporous Cu-MOF nanoplates using ILs.[51] The resulting material had high crystallinity and combined the pro-

Table 1 Advantages and disadvantages of different MOF synthesis methodologies/strategies

Synthesis method	Advantages	Disadvantages
Solvothermal/hydrothermal 	○ High crystallinity[63] ○ Control of morphology[64,65] ○ Control of particle size[66]	○ Long synthesis times[30] ○ Use of organic solvents[67]
Non-solvothermal 	○ Energy saving by using room temperature[68,69]	○ Low yield[70] ○ Use of organic solvents[26]
Sonochemical/ultrasound 	○ Control of crystal growth[33] ○ High yield[71,72] ○ Short synthesis times[73]	○ Use of organic solvents[74]
Electrochemical 	○ Easy to scale[75] ○ Short synthesis times[76,77]	○ Reduction in A_{BET}[39,41] ○ Use of organic solvents[78]
Microwave-assisted 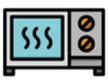	○ Short synthesis times[79,80]	○ Small crystal size[44] ○ Use of organic solvents[21]
Ionothermal 	○ Ionic liquids replace organic solvents[81,82]	○ Reduction in A_{BET}[83]
Mechanochemical 	○ Solvent-free[57,84] ○ Short synthesis times[85]	○ Difficult to control morphology and particle size[86]

perties of a mesoporous material with small particle sizes. In 2014, Liu *et al.* introduced an innovative approach for immobilizing ILs into ZIF-8 membranes. ZIF-8's inherent hydrophobicity and ability to act as a template with an ionic liquid effectively confined the IL within the membranes and reduced leaching when exposed to water.[52]

- **Mechanochemical synthesis** uses mechanical energy, such as compression, shear or friction, to facilitate chemical transformations. This technique is particularly relevant to green chemistry, as it eliminates or reduces the need for solvents.[53] Mechanochemical synthesis is a promising method for the large-scale production of MOFs due to its advantages, such as solvent-free reactions at room temperature and relatively short reaction times of 10 to 60 min. Ball milling is the primary process used to crush precursors between balls, resulting in bond breakage, defects and increased reactivity.[54,55] Over the past decade, mechanochemical synthesis of MOFs has performed well compared with conventional techniques, as shown in reviews[56] or book chapters.[57] Although ball milling is widely used, it has limitations such as sample damage and non-uniform mixing. Other methods, such as RAM, can overcome these problems. RAM uses low-frequency, high-intensity acoustic energy to gently mix materials without physical contact with balls.[58] Titi *et al.* demonstrated that the RAM technique is more advantageous than ball milling for synthesizing ZIF-L, ZIF-8 and HKUST-1.[59] RAM enables larger batches to be synthesized while retaining control over product composition and particle size.

MOF formation, layout and shape are affected not only by the building blocks, but also by factors such as solvent, pH, temperature, reagent concentration, reaction time, molar ratios, counter ions and pressure. These factors fall into two categories (Fig. S3b†): (1) compositional parameters – solvent, pH, molar ratios, counter ions, and concentration; and (2) process parameters – pressure, time, and temperature.[60] In assembly processes, solvents coordinate with metal ions or integrate into the lattice.[61] Although they do not integrate directly into the MOF, solvents play a role in structure orientation and crystal growth. The choice of solvent influences ligand deprotonation, which in turn has an impact on the MOF structure.[60] For instance, using different solvents, Banerjee *et al.* revealed various crystal structures in MOFs synthesized with magnesium and 3,5-pyridine dicarboxylic acid (PDC).[62] Water coordinated best with magnesium, but the maximum A_{BET} value achieved was 52 $m^2\ g^{-1}$. Acidity/basicity has a significant influence on the crystallization and growth of inorganic–organic composite materials. pH has an impact on ligand deprotonation, strengthening the bond between ligands

and metal ions through pH adjustments.[60] Temperature also has a significant impact on MOF characteristics, as demonstrated by Biemmi *et al.*, who found that temperature variations (from 75 to 180 °C) altered the morphology and purity of HKUST-1.[29]

Synthesis time has a significant effect on MOFs' crystal size, as shown by Xu *et al.* who synthesized MOF-808 at 120 °C using $ZrCl_4$/BTC (3 : 1 ratio) for 36–96 h.[87] During the first 36–72 h, A_{BET} and micropore volume increased from 1052 to 2177 $m^2\ g^{-1}$ and from 0.30 to 0.72 $cm^3\ g^{-1}$, respectively. After 72–96 h, A_{BET} and micropore volume decreased to 968 $m^2\ g^{-1}$ and 0.28 $cm^3\ g^{-1}$, respectively. Suresh *et al.*[88] studied various process parameters to optimize MOF synthesis for H_2 storage. The researchers investigated the effect of reagent concentration, temperature and reaction time on crystal size distribution. Shorter reactions (12–18 h) at higher temperatures (110–150 °C) produced cubic crystals with a wide size distribution (200–1300 μm), whereas longer reactions (24–72 h) at lower temperatures (60–90 °C) produced crystals with a narrower size distribution and with a 15% reduction in A_{BET}.

2.2. MOF characterization

Characterizing MOFs is a crucial step in understanding their structure and properties. The main techniques to characterize a MOF are as follows: X-ray diffraction (XRD), to identify the crystal structure and unit cell dimensions; scanning electron microscopy (SEM), which provides images of surface morphology and particle size distribution (Fig. 2a); thermogravimetric analysis (TGA), to determine thermal stability and weight loss behavior upon heating (Fig. 2c); gas sorption analysis, to determine pore volume, pore size distribution and the surface area (Fig. 2b); Fourier-transform infrared spectroscopy (FTIR), to identify functional groups present; and elemental analysis to find out the composition of the MOF, usually in terms of carbon, nitrogen and oxygen contents. These analyses provide valuable information on the physical and chemical properties of MOF materials. This information is crucial for understanding their potential applications.

Other promising but less explored techniques are described in Fig. 2. Confocal fluorescence microscopy has the unique ability to capture three-dimensional images at the level of individual crystals (Fig. 2e), while offering the sensitivity needed to investigate the initiation of defect formation. Raman spectroscopy provides detailed information on the molecular vibrations and vibrational modes present in a material, which can be useful for studying the structure, composition and properties of MOFs. Confocal laser scanning microscopy can be used to observe the stability of MOF hybrids if they contain a fluorescent component such as carbon dots (CDs). XPS spectra are used to analyze the elemental composition and chemical state of a material's surface, to confirm the doping of a MOF (Fig. 2d), and nuclear magnetic resonance (NMR) can be used to study the structure of organic components in MOFs and the interaction between organic molecules and metal ions (Fig. 2f).

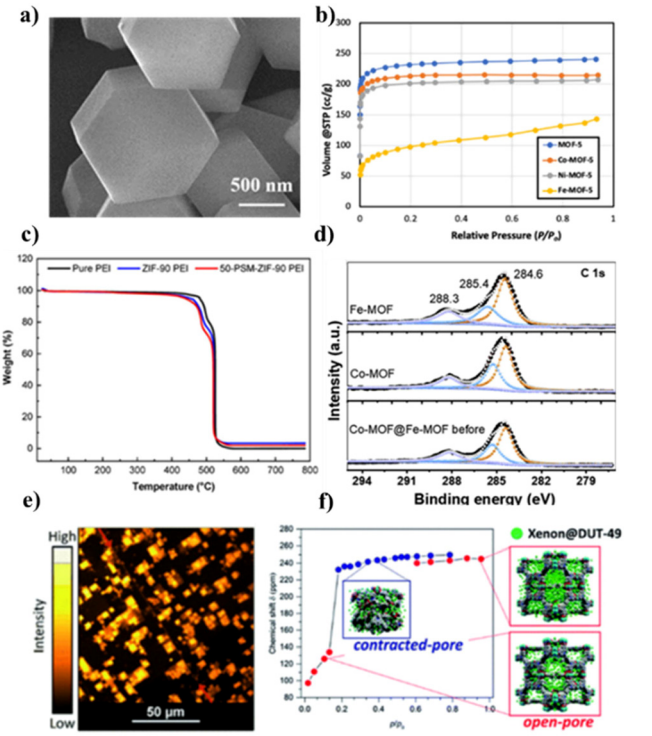

Fig. 2 Main MOF characterization techniques: (a) SEM images of ZIF-8 (reproduced from ref. 89 © 1996–2024 MDPI); (b) nitrogen adsorption isotherms at −196 °C of MOF-5 and doped MOF-5 (reproduced from ref. 90 © 1996–2024 MDPI); (c) TGA of pure PEI, ZIF-90 PEI and 50-PSM-ZIF-90 PEI membranes (reproduced from ref. 91 © 1996–2024 MDPI); (d) XPS spectra of Fe-MOF, Co-MOF, Co-MOF@Fe-MOF, and the hybrid MOF (reprinted with permission from ref. 92; Copyright © 2024 with permission from Elsevier. Also Lancet special credit, reprinted from The Lancet from ref. 92; Copyright © 2024 with permission from Elsevier); (e) confocal fluorescence imaging of defects in a MOF-5 single-crystal (reproduced from ref. 93 © 1999–2024 John Wiley & Sons, Inc. or related companies); (f) chemical shift of xenon adsorbed in DUT-49 at −73 °C measured during the adsorption experiment (red symbols indicate DUT-49op signals; blue symbols indicate DUT-49cp signals) (reprinted with permission from ref. 94; Copyright(2017) American Chemical Society).

3. Fundamental properties and performance of MOFs for hydrogen storage

The characteristics required to design the ideal MOF for H_2 sorption have been reported in several studies.[15,95,96] In general, MOFs must have a high surface area and a large number of relatively small, interconnected pores to maximize H_2 adsorption. Low-density MOFs are disadvantageous as they can lead to weak H_2–H_2 interactions in the channels, reducing adsorption capacity. Additionally, volumetric H_2 storage capacities are also reduced. When used near room temperature, the inner surface of MOFs must feature local polar groups to enhance interactions between MOFs and H_2 molecules, and this requirement relates specifically

to the properties of the organic linker used in MOF synthesis.

3.1. Specific surface area

H_2 is adsorbed on the surface of the material and stored in the pores (physisorption). In general, micropore volume is directly related to the surface area of a material. Consequently, to enhance H_2 adsorption capacity at −196 °C, it is necessary to increase both specific surface area (SSA) and micropore volume within the MOF. Fig. 3a shows a limitation of the BET method in representing excess H_2 uptake in wt% (at −196 °C) of MOFs as a function of their A_{BET}. It demonstrates that for very high A_{BET}, Chahine's heuristic rule is not valid, as the BET method accounts for pore volume more than SSA. The isosteric enthalpy of adsorption ($(-\Delta H)_{ads}$) exhibits a linear decrease with increasing average pore diameter (Fig. 3b). This phenomenon is attributed to stronger adsorption forces in narrow pores, due to overlapping van der Waals forces. The presence of 1.5 to 2.5 nm pores has been shown to significantly enhance H_2 storage capacity at high pressures. However, nanopores smaller than 1.5 nm are found to be the most efficient for H_2 storage at all pressure levels.[97] H_2 interactions with MOFs can be enhanced by reducing pore size, with the optimum size corresponding to the kinetic diameter of the H_2 molecule (0.289 nm),[98] although porous materials with a unimodal PSD of around 0.3 nm and high surface areas are difficult to obtain.

Fig. 3c illustrates a linear relationship between SSA and pore volume for different MOF families. This behavior was previously reported by Gómez-Gualdrón *et al.*, who calculated the A_{BET} of microporous and mesoporous MOFs.[99] In Fig. 3d, absolute volumetric H_2 adsorption is plotted against absolute gravimetric H_2, showing that for MOFs with high BET areas, a plateau in H_2 uptake on a volumetric basis is reached. The latter was determined using the following equation, deduced

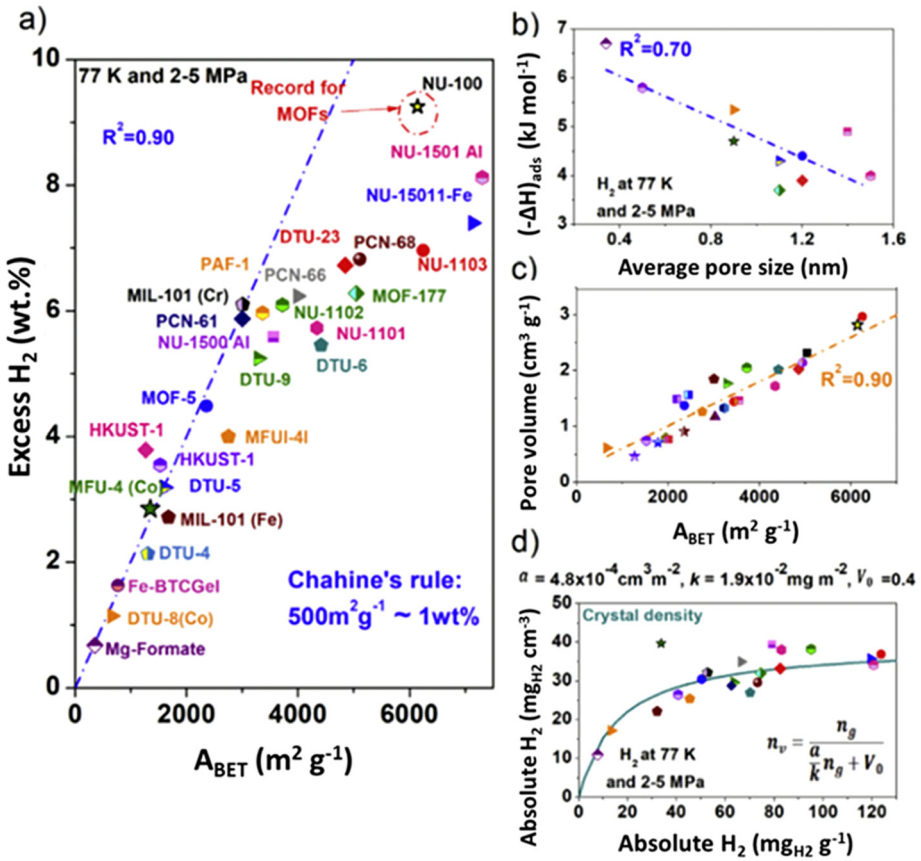

Fig. 3 (a) Excess H_2 uptake at −196 °C and 2–7 MPa of metal–organic frameworks (MOFs) reported in recent studies (▶◆◆⬟●◑●◑▶) ref. 111, (▶▶★◑◒) ref. 104, (●●●) ref. 112, (●▶■) ref. 113, (☆) ref. 8, (▶◆●) ref. 114, (●●⬟★ ★◧★▲◨■) ref. 115, (◑■) ref. 116. (a) Chahine's rule (dotted line) applied to MOFs; (b) isosteric heat of adsorption $(-\Delta H)_{ads}$ as a function of average pore size; (c) evolution of pore volume with A_{BET}; (d) volumetric *versus* gravimetric absolute hydrogen uptake of porous materials using the density of the single crystal for its calculation for MOFs: (⬟◆◆⬟●◑●◑▶) ref. 111, (▶▶★◑◒) ref. 104, (●●●) ref. 112, (●▶■) ref. 113, (☆) ref. 8, (▶◆●) ref. 114. The green line in (d) corresponds to the model proposed by Balderas-Xicohténcatl *et al.* in ref. 101. The absolute uptake from the excess reported data was calculated using REPROF software to calculate the density of H_2 gas and assuming that the volume of the adsorbed phase volume is equal to V_{pore}. (reprinted with permission from ref. 117; Copyright © 2024 with permission from Elsevier. Also Lancet special credit, reprinted from The Lancet from ref. 117; Copyright © 2024, with permission from Elsevier).

from H_2 uptake on several MOFs, at −196 °C and in a pressure range of 2 to 2.5 MPa:[100,101]

$$n_v = \frac{n_g}{\frac{\alpha}{k} n_g + V_0}.$$

In this equation, n_v and n_g are the volumetric and gravimetric absolute uptakes, respectively; α represents the slope of the relationship between volumetric absolute hydrogen uptake (measured at −196 °C and 2.0–2.5 MPa) and the volumetric surface area, which is derived from single-crystal densities; κ is the H_2 surface density, and V_0 is the density of the MOF single-crystal.

The ability of any adsorbent to store H_2 (wt%) is closely linked to its SSA. Moreover, there is a linear correlation between the wt% of H_2 stored and the BET area.[102] The shapes of N_2 isotherms observed for physisorption on MOFs, which are often type I with minimal or no hysteresis, indicate the presence of well-defined microporous structures. The pronounced rise at very low p/p^0 is attributed to adsorbent–adsorbate interactions in these narrow micropores.[20,103]

3.2. Isosteric enthalpy of hydrogen adsorption

In gas storage, especially in H_2 storage on MOFs, van der Waals forces are considered the main gas–adsorbent interaction and contribute to the decrease in H_2 storage pressure in the system.[19] For practical storage applications, a reversible mechanism is required for the adsorption and release of H_2 from its storage material. The low physisorption of H_2 on MOFs offers an advantage in this regard, as it allows H_2 to be adsorbed on pore surfaces within the MOF and readily released on demand. However, the challenge lies in the low $(-\Delta H)_{ads}$ of H_2 on most known MOFs. For optimum hydrogen storage and release cycles at room temperature, an adsorbent should have a $(-\Delta H)_{ads}$ between 15 and 25 kJ mol^{-1}. This range is crucial when considering the system's operating pressures. The release pressure corresponds to the pressure after most of the hydrogen has been released from the adsorbent. If $(-\Delta H)_{ads}$ is too high, desorption will require higher temperatures or lower pressures, which may not be practical under ambient conditions. Conversely, the storage pressure is the pressure at which the adsorbent is fully loaded with hydrogen. If $(-\Delta H)_{ads}$ is too low, the adsorbent may not retain hydrogen effectively at this pressure, leading to inefficient storage.[104–106] Unfortunately, the majority of MOFs exhibit $(-\Delta H)_{ads}$ values between 5 and 12 kJ mol^{-1}.[107]

Recent studies have provided H_2 adsorption isotherms for more than 30 MOFs, covering a pressure range of up to 1 bar.[108] Among the challenges posed by these porous materials for H_2 adsorption are: achieving high H_2 uptake under ambient conditions, improving the kinetics of H_2 adsorption and desorption, and increasing material stability and durability. While MOFs exhibit significant H_2 uptake at cryogenic temperatures, reaching up to 99.5 mg g^{-1} (approximately 9 wt%) at 56 bar and −196 °C,[8] their storage capacities at room temperature are generally less than 1 wt%.[95] This limitation is due to the weak interaction, typically ranging from −12 to −5 kJ mol^{-1}, between H_2 molecules and MOFs.[109] However, as temperature increases, H_2 storage capacity decreases significantly, and none of the existing MOFs currently meet the target set by the US DOE at room temperature.[107] According to the US DOE, materials must have a minimum H_2 uptake capacity of 5.5 wt% under moderate temperature and pressure conditions.

The amount of energy released by interactions between the MOF surface and H_2 molecules can be determined by analyzing H_2 adsorption isotherms obtained at least at two distinct temperatures, typically −196 and −186 °C. This is achieved by fitting the experimental data to either the virial equation or the Langmuir–Freundlich equation.[107] Bae and Snurr[110] conducted a study of H_2 storage and release with a MOF at pressures between 1.5 and 120 bar using Grand Canonical Monte Carlo simulations. The aim was to determine the ideal value of $(-\Delta H)_{ads}$ to maximize H_2 delivery. The simulations revealed that the optimum $(-\Delta H)_{ads}$ value for this purpose is approximately 20 kJ mol^{-1}, in agreement with other works.[104–106]

Linker functionalization seems to be an effective approach for enhancing the H_2 adsorption enthalpy of MOFs and improve hydrogen storage capacity, either through direct modification or post-synthetic modification of the linker.[118] In this context, Han *et al.* enhanced UiO-66 by incorporating dihydroxy and dialkoxy groups into its linker. This modification resulted in UiO-66-$(OCH_2CH_3)_2$, which exhibited a 98.3% improvement in performance compared to the unmodified UiO-66.[119]

The incorporation of different functional groups such as $-CH_3$, $-NH_2$, –OH, and –Br into the organic linker results in a series of isoreticular MOFs whose fundamental framework remains unchanged and which can effectively increase the $(-\Delta H)_{ads}$.[120] The potential of linker functionalization can be seen with tetrazolate-based ligands, which generate a series of robust, microporous materials. Dinca *et al.*[121] successfully synthesized nitrogen-rich MOFs using 1,4-benzeneditetrazolate as an organic linker, achieving H_2 storage densities of up to 1.46 wt% at ambient pressure. Wang *et al.* covalently modified MOFs (IRMOF-3, UMCM-1-NH_2 and DMOF-1-NH_2) with a series of anhydrides or isocyanates: storage adsorption capacities (gravimetric and volumetric gas uptakes) and $(-\Delta H)_{ads}$ demonstrated that post-synthetic covalent modifications can greatly enhance the sorption affinity of MOFs for H_2.[122]

Another way to strengthen the interaction between hydrogen and MOFs is through the introduction of unsaturated metal sites. Developing these sites effectively enhances the enthalpy, thereby improving hydrogen storage performance. This is commonly achieved by removing coordinated solvents using methods such as heating, vacuum heating, or supercritical drying.[123] Sengupta *et al.* synthesized a robust Cu(I)-based MOF, called NU-2100, which contains open metal sites. To access these open metal sites, the MOF underwent an activation process. The study concluded that the activated MOF exhibited a high enthalpy of adsorption of 30 kJ mol^{-1}.[124]

3.3. Hydrophobicity

To achieve optimal performance and recyclability in H_2 storage, one of the most important objectives is to improve the water stability of MOFs, which are sensitive to moisture.[125,126] When MOFs are exposed to moisture from the air, the organic ligands in the framework are replaced by water molecules. This substitution disrupts the metal–linker bonds, which are generally the weakest points of the MOF structure. As a result, the MOF structure partially decomposes, leading to a reduction in SSA.[127,128] There are two approaches for addressing this challenge. The first is the direct synthesis of water-stable MOFs, which can be achieved by incorporating non-polar functional groups into the organic linkers.[129,130] The second method involves post-synthetic modifications, which include encapsulation of hydrophobic guest molecules in the MOF's pores and channels,[131] as well as functionalization of the MOF's external surface.[132] Qian *et al.* have synthesized a hydrophobic DUT-4 by a facile solution-immersion approach. After exposure to aqueous solutions, DUT-4 treated with a hydrophobic coating successfully preserved its crystal structure, morphology, surface area and H_2 uptake capacity.[133]

3.4. Thermal conductivity

Thermal conductivity within MOFs is a crucial but often overlooked issue in numerous adsorption-based applications, including gas storage and separation. In adsorptive gas storage applications, the heat generated by exothermic gas adsorption can potentially lead to a considerable increase in temperature (hot spots) and decrease the MOF's adsorption capacity if not promptly dissipated.[134] Effective thermal conductivity is a crucial parameter for assessing the rate at which adsorption heat dissipates and for devising strategies to maintain a lower temperature in a fuel storage tank while it is being filled with hydrogen.[135] Islamov *et al.* reported that MOFs exhibit enhanced thermal conductivity when they have high densities (>1.0 g cm^{-3}),[136] small pores (<1 nm)[137] and four-connected metal nodes.[138] The highly porous nature and low density of MOFs prevent efficient phonon transport[139] and result in low thermal conductivities (<2 W m^{-1} K^{-1}).[140]

3.5. Tap density

The use of MOF powders in large industrial reactors can lead to pressure drops, clogs and complex handling. To mitigate these issues, MOF powders are shaped into defined structures using various methods such as pelletization, extrusion, granulation, spray-drying or 3D printing.[141] This shaping process usually involves the incorporation of binders to improve the mechanical stability of the pellets, which is highly advantageous. Binders generally fall into two categories: organic binders, which include starch, cellulose and polyvinyl alcohol, and inorganic binders, such as clay, silica and graphite.[142,143] Factors such as pore collapse, pore blocking and amorphization of the crystalline structure can lead to a reduction in the storage capacity of compressed MOFs.[144] Packing efficiency is a key factor in determining the H_2 storage capacity of MOFs. Research on the packing density on real MOF samples with different crystal shapes and sizes is the most effective method for gaining insight into packing efficiency. The choice of the synthesis method and the precise adjustment of various parameters (such as temperature, synthesis time, pH, concentration, *etc.*) are essential in determining the size and shape of the resulting crystal.[145] Suresh *et al.* designed a strategy to improve packing efficiency and significantly increase the volumetric storage density of H_2 gas by controlling the crystal morphologies and crystal size distributions for MOF-5.[88] This strategy has the potential to minimize the structural damage when the MOF is compacted, thereby maximizing the H_2 storage capacity compared with compacted commercial MOF-5. The synthesis method chosen can also alter the crystal size. For example, Leng *et al.* synthesized MIL-101(Cr) by mechanosynthesis, obtaining crystals between 40 and 200 nm, in contrast to the 300 to 500 nm crystals achieved by solvothermal methods.[146] The choice of the appropriate synthesis route thus plays an important role in MOF crystal size, which can result in better packing.[88]

3.6. Thermal stability

The thermal stability of a MOF refers to its ability to avoid irreversible changes to its structure when heated to a specific temperature.[147] Yuan *et al.* highlight that the stability of MOFs is strongly influenced by various factors, such as the framework structure, particle size, crystal defects, and operational conditions,[126] but overall, two factors have been identified to contribute the most to the stability of MOFs: the properties of the linkers and the metal–linker bonds.[148]

Recognizing the key influence of linkers on the thermal stability of MOFs, Mohamed *et al.* studied the impact of using functionalized linkers in MOF-5. They concluded that non-functionalized linkers exhibit greater thermal stability.[149]

The thermal stability of amorphous regions of MOFs is generally much lower than that of crystalline regions of similar composition.[150] During the heat treatment process, degradation of MOF structures can lead to amorphization, melting, cluster dehydration or dehydrogenation of the organic ligand.[151–153] Increased thermal stability results in more stable and durable materials.

4. Hydrogen adsorption on MOFs and their hybrids

MOF hybrids are materials that combine MOFs with other substances to create new materials with improved properties or functionalities.[163] The aim of combining MOFs with alternative materials is to overcome the limitations of MOFs, such as low stability, poor mechanical properties or high production costs. In addition, the hybrids can be tailored to specific applications such as H_2 capture, with improved efficiency and performance.[164–167] Table 2 presents the advantages and disadvantages of certain types of MOF hybrids. The following sections provide a detailed description of each selected hybrid.

Table 2 Advantages and disadvantages of different MOF hybrids

Hybrids	Advantages	Disadvantages
Interpenetrated MOFs (IMOFs) 	○ Improved framework stability[154] ○ Larger adsorption selectivity[155]	○ Surface area potentially decreased[156]
MOF-on-MOF 	○ Properties of different MOFs combined[157]	○ Difficult synthesis[11]
MOF/carbon-based materials 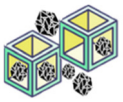	○ Increased A_{BET}[158] ○ Increased H_2 adsorption (−196 °C)[159] ○ Increased thermal conductivity[143]	○ Decreased crystallinity[159]
MOF/metal particles and ions 	○ Increased H_2 adsorption (25 °C)[160] ○ Enhanced adsorption enthalpy[161]	○ Decreased surface area[162]

4.1. MOF@MOF hybrids for hydrogen adsorption

MOF@MOF hybrids refer to materials composed of two MOFs combined into a single system. By combining two MOFs, it is possible to achieve various advantages aimed at increasing H_2 adsorption capacity, such as reducing pore size, increasing gas selectivity and improving MOF stability.[168,169] Fig. 5 shows the influence of combining two MOFs on H_2 adsorption at −196 °C and 25 °C. Combining MOFs by interpenetration can have a reducing effect on the SSA of the resultant hybrids. However, all samples show an increase in H_2 adsorption.

4.1.1. Interpenetrated MOFs (IMOFs). The presence of large pore spaces in the MOF system can be associated with instability and subsequent collapse of the structure. To solve this problem, interpenetration (also called catenation or interweaving) can be used, as it allows the entanglement of two identical MOFs (homo IMOFs) or two different MOFs (hetero IMOFs) that are not directly connected but cannot be separated without breaking bonds[154,170–172] (Fig. 4). Interpenetration minimizes vacant zones and has the potential to significantly improve framework stability. It allows empty spaces to be occupied and generates repulsive forces that prevent individual networks from collapsing. Consequently, the synthesis of MOFs with adjustable pore sizes using elongated organic linkers poses considerable challenges, as the formation of interwoven frameworks should be preferred to improve stability.[173] Catenation can be used to produce materials with fine pores and enhance adsorption heat by increasing the overlap of attractive potential between opposing pore walls. As a result, the interpenetrated framework shows a significant reduction in pore size, resulting in stronger interaction with H_2 molecules.[100]

Ma *et al.* (2007) investigated the effect of interpenetration on H_2 adsorption in PCN-6, a porous coordination network. The N_2 adsorption isotherm at −196 °C shows that the non-

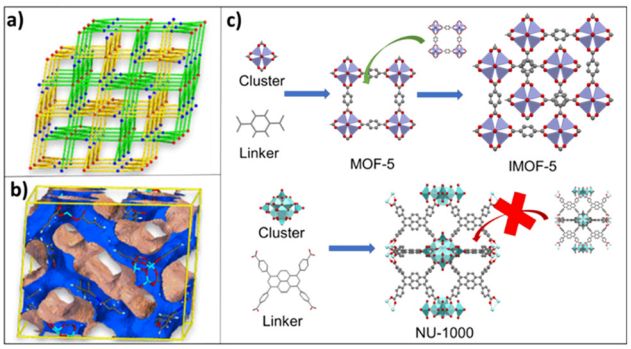

Fig. 4 (a) Topological representations of interpenetration along the *a*-axis; (b) the 1D channel viewed along the *a*-axis (a) and (b) reproduced from ref. 174, with these figures having been published in *CCS Chem.* [2022]; [Ultrahigh hydrogen uptake in an interpenetrated Zn_4O-based metal–organic framework] is available online at https://10.31635/ccschem.021.202000738; (c) simplified topology of an interpenetrated MOF-5 and the impossibility of NU-1000 interpenetration.

interpenetrated material has a Langmuir surface area of 2700 $m^2\ g^{-1}$, while the interpenetrated material has a Langmuir surface area of 3800 $m^2\ g^{-1}$, representing a 41% increase. Interpenetration resulted in a 133% increase in volumetric H_2 uptake (3.94 kg m^{-3} for non-interpenetrated frameworks *vs.* 9.19 kg m^{-3} for interpenetrated frameworks) and a 29% increase in gravimetric H_2 uptake (1.35 wt% for non-interpenetrated frameworks and 1.9 wt% for interpenetrated frameworks).[185]

Jiang *et al.* also used a MOFMC for H_2 storage, an interpenetrated MOF-5@Multi-Walled Carbon Nanotubes (MWCNTs), called Int-MOFMC-meso.[175] The latter was able to store 2.02 wt% H_2 at −196 °C under 1 bar. This value is higher than those obtained for the aforementioned MOFMC materials and indicates better thermal and moisture stability. However, the

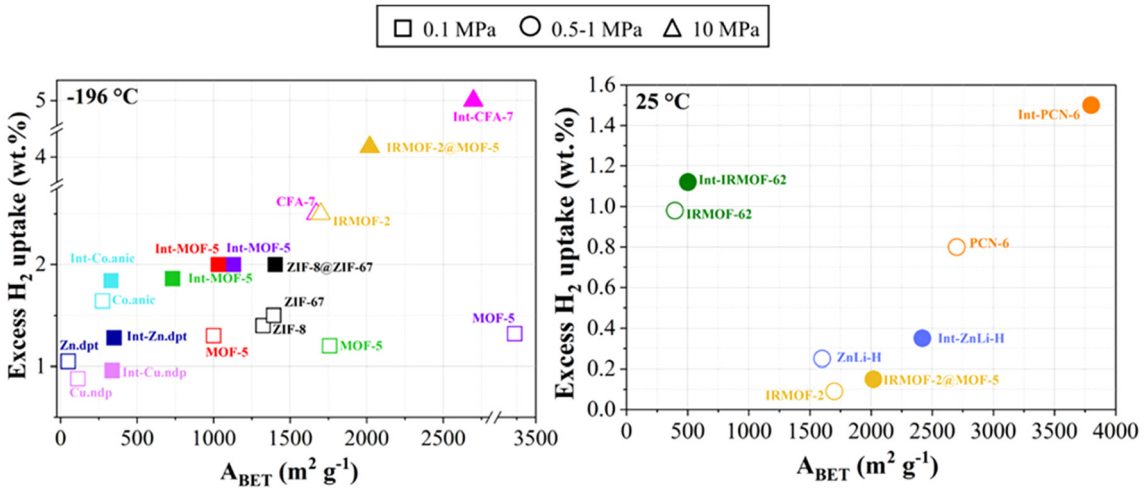

Fig. 5 Excess H_2 storage capacities of MOFs and their MOF@MOF hybrids at −196 °C (left) and 25 °C (right). (□ ■ ref. 175); (□ ■ ref. 176); (□ ■ ref. 177); (□ ■ ref. 178); (□ ■ ref. 174); (△ ▲ ref. 100); (○ ●, △ ▲ ref. 179); (□ ■ ref. 180); (□ ■ ref. 181); (○ ● ref. 182); (○ ● ref. 183); (○ ● ref. 184).

A_{BET} was significantly lower than that of previous MOFMCs: 805 $m^2\ g^{-1}$. According to the authors, the pores were not filled with zinc species or solvent, but it was the presence of an interpenetrated structure and the unsaturated metal site present on the mesopore surface that improved H_2 storage performance, even with a lower A_{BET}.[175]

4.1.2. MOF-on-MOF. Extensive studies on MOFs have led to the development of a promising class of hybrid materials known as MOF-on-MOF, as shown in Fig. 6a. The left-hand side of the figure shows the original MOF seed, while the right-hand side displays the MOF grown as a secondary layer. This demonstrates how two or more MOF units are combined to create a new hybrid material.[186] This approach results in unique properties that can be customized for specific applications. This method enables the distinct properties of different MOFs to be combined, such as high porosity, specific functionality or catalytic activity, and can also improve the stability and mechanical properties of the resulting material.[187]

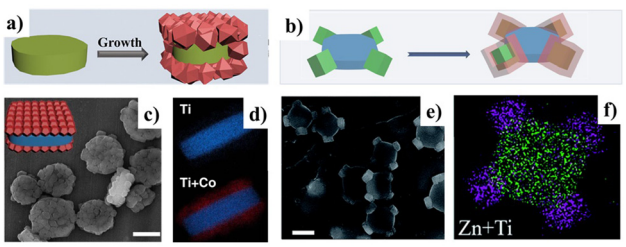

Fig. 6 (a) Scheme of a binary MOF-on-MOF heterostructure (reproduced from ref. 157; Copyright © 1999–2024 John Wiley & Sons, Inc. or related companies); (b) scheme of a ternary MOF-on-MOF heterostructure (ref. 188, reprinted with permission as indicated in the Terms and Conditions of the license); (c) SEM image of MOF MIL-125@ZIF-67 (ref. 188, reprinted with permission as indicated in the Terms and Conditions of the license); (d) element mapping image of MIL-125@ZIF-67 (reproduced from ref. 188, reprinted with permission as indicated in the Terms and Conditions of the license); (e) SEM image of MIL-125@ZIF-8 (reproduced from ref. 189 with permission from the Royal Society of Chemistry); (f) elemental mapping image of MIL-125@ZIF-8 (reproduced from ref. 189 with permission from the Royal Society of Chemistry).

In general, there are two main approaches for synthesizing MOF-on-MOF structures. The first approach involves a two-step process, with pre-synthesized host MOFs used as seeds in the first step, and guest MOFs are grown on them in the second step to form MOF-on-MOF structures. The second approach involves a one-pot process that controls the nucleation and growth kinetics of both host and guest MOFs.[11]

The growth of guest MOFs can occur *via* five mechanisms, namely: epitaxial, heteroepitaxial, surfactant-assisted, nucleation kinetic-guided, and ligand/metal ion-exchange growth.[11,190] However, current MOF-on-MOF systems mainly focus on compositions consisting of two or more components[188] (Fig. 6a and b). For example, Ikigaki *et al.* reported a ternary MOF-on-MOF copper structure,[191] composed of an oriented MOF-on-MOF film, with lower and upper MOF layers. The films were created by epitaxially matching the interface and "one-pot" and liquid-phase epitaxy methods for the layers with copper-based reactants.

To assess the interaction between MOFs involved in MOF-on-MOF hybrids, their structures can be studied using SEM images, and element mapping enables their structures to be investigated through morphology analysis of two or more MOF varieties (see Fig. 6c–f). By integrating the aforementioned properties of various MOFs into MOF-on-MOF systems, it is possible to control gas adsorption capacity and selectivity while improving adsorbent stability.[11]

Li *et al.* developed a MOF-on-MOF structure specifically designed for gas adsorption. The structure comprised a core composed of a mixture of bio-MOF-11 and bio-MOF-14, while a bio-MOF-14 shell encapsulated the core. Water stability testing confirmed that the hydrophobic bio-MOF-14 shell pro-

tected the water-sensitive core from degradation. The resulting MOF-on-MOF hybrids displayed selective gas storage properties and improved water stability.[192]

Panchariya *et al.* synthesized two variants of zeolitic imidazolate frameworks (ZIFs), the core–shell ZIF-8@ZIF-67 and the ZIF-67@ZIF-8. Both exhibited high H_2 storage values, reaching 2.03 wt% for ZIF-8@ZIF-67 and 1.69 wt% for ZIF-67@ZIF-8. Under −196 °C and 1 bar conditions, the H_2 storage capacity of the hybrids improved by 41% and 18% compared with their ZIF-67 and ZIF-8 parents, respectively. According to the authors, these values of H_2 uptake indicate that the unique structural features of the core–shell materials, such as the confinement of a porous structure within another one and their elemental heterogeneity, were the main reasons. The best material in terms of H_2 storage, the core–shell ZIF-8@ZIF-67, had an A_{BET} of 1402 $m^2\ g^{-1}$, higher than that of ZIF-8 with 1324 $m^2\ g^{-1}$ and ZIF-67 with 1392 $m^2\ g^{-1}$. The authors suggested that this increase was due to the well-developed ZIF-67 shell over the ZIF-8 core, which did not block the ZIF-8 pores. Nevertheless, the core–shell ZIF-67@ZIF-8 was the second-best performing and had a lower A_{BET} than its ZIF parents, 1272 $m^2\ g^{-1}$, indicating that the most important variables were the distinct surface and porosity characteristics of the core–shell topologies.[180] The results underscore the potential of MOF-on-MOF systems for efficient gas storage applications.

4.2. MOF hybrids with carbon-based materials or metals

The exceptional porosity and versatility of MOFs enable the synthesis of hybrids with a variety of materials, including polymers, graphene oxide, carbon nanotubes, metal nanoparticles, *etc*.[170,193] This can be achieved by growing MOFs on the surface or in the pores of other substrates or by incorporating additional materials into MOF cavities. As a result, hybrids can exhibit a combination of the properties of both components or even acquire new functionalities, such as water stability, or even improved mechanical properties.[194,195]

Fig. 7 shows the various possible synthesis approaches for obtaining a MOF hybrid, including covalent modification at metal nodes (Fig. 7a) or organic ligands (Fig. 7b), encapsulation (Fig. 7c), layer-by-layer deposition (Fig. 7d), or nucleation in the presence of other materials (Fig. 7e).[196]

MOF hybrids can be synthesized by various methods, such as *in situ* growth, post-synthetic modification and physical mixing.[180,197,198]

- ***In situ* growth**: In this approach, carbon-based materials or metals are incorporated into the MOF structure during MOF synthesis. These materials can therefore serve as nucleation sites for MOF crystal growth, and their presence can influence the morphology, structure and properties of the resulting MOF hybrid. The designation for this approach is MOF@A, with "A" being another material that forms a non-covalent interaction between the two components. Alfe *et al.* used graphene-like (GL) materials to prepare HKUST-1@GL, MIL-96(Al)@GL and MIL-101(Fe)@GL by *in situ* growth. The materials obtained achieved good selectivity for CO_2 over CH_4 using MOF@GL

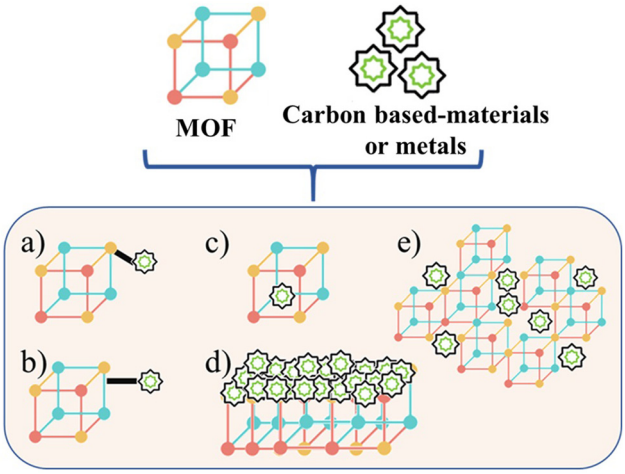

Fig. 7 Scheme of hybrid materials based on MOFs and carbons or metals: (a) covalent modification at metal nodes; (b) covalent modification at organic ligands; (c) encapsulation; (d) layer-by-layer deposition; and (e) nucleation in the presence of other materials (adapted from ref. 196).

hybrids.[199] Pt and Au nanoparticles were used as nucleation sites during ZIF-8 synthesis, enabling Pt and Au nanoparticles to be encapsulated.[200] He *et al.* synthesized MOF-5@Au[201] and Liu *et al.* synthesized UIO-66@Pt using a one-pot method in which the nanoparticles and MOFs were synthesized simultaneously.[202]

- **Post-synthetic modification**: In this approach, pre-synthesized MOFs are modified by introducing carbon-based materials or metals onto the MOF surface or into its pores once MOF synthesis has been completed. Post-synthetic modification methods allow other materials with specific properties or functionalities to be introduced into MOFs without altering the MOF structure.[203]

Covalent modifications encompass both coordinated covalent modifications of metal clusters and covalent modifications of ligands. By employing covalent modification techniques, it is possible to synthesize MOF hybrids with small molecules, metals/metal clusters, covalent organic frameworks (COFs), polymers and graphene.[196,203] Rao *et al.* developed a composite membrane combining graphene oxide (GO) and UiO-66-NH_2 by tethering UiO-66-NH_2 to GO surfaces. The covalent attachment of UiO-66-NH_2 with GO enabled the creation of a continuous proton transfer channel, contributing to the high performance of the composite membrane.[215]

Post-synthetic modification also includes techniques such as coating, layering and other methods that do not rely on the formation of covalent bonds. For instance, Chen *et al.* developed a material comprising perovskite quantum dots (QDs) encapsulated in HKUST-1 by immersing HKUST-1 thin films in solutions containing QD precursors. QDs of 1.5–2 nm matched the pore size of HKUST-1 and the resulting material improved its stability under 70% relative humidity, whereas QDs alone decomposed under the same conditions.[216] Villajos *et al.* obtained a ZIF-8@Pd hybrid by synthesizing Pd nano-

particles in the presence of commercial ZIF-8[212] and Hu *et al.* followed a similar route to obtain HKUST-1@Pd.[209]

- **Physical mixing:** This approach involves simply mixing MOFs and carbon-based or inorganic materials without any covalent or coordination bonds between them. This approach is relatively simple and straightforward but may result in phase separation or weak interactions between MOFs and other materials. Otal *et al.* stated that the inherent characteristics of MOFs, including crystallinity, structure and porosity, were maintained even after the modification of pre-synthesized MOFs.[217] Some studies confirm a significant improvement in H_2 sorption capacities when MOFs are mixed with carbon-based materials.[163,218] Prasanth *et al.* clearly demonstrated a substantial improvement in the H_2 sorption capacities of MIL-101 samples through the incorporation of Single-Walled Carbon Nanotubes (SWCNTs). H_2 sorption capacities increased from 6.4 to 9.2 wt% at −196 °C and 6 MPa and from 0.2 to 0.6 wt% at 25 °C and 6 MPa.[218] In their feature article, Szczęśniak *et al.* studied the incorporation of GO into different MOF matrices such as HKUST-1 and MIL-101(Cr). They observed that the presence of GO can significantly increase their surface area and influence their morphology and structure. The dense atomic structure of GO contributes to stronger dispersion interactions and a greater number of unsaturated coordination bonds when combined with MOFs, which is crucial for improving adsorption properties.[163]

4.2.1. MOF hybrids with metal particles and ions for hydrogen storage. One of the most attractive structural features of some MOFs is coordinative unsaturation, which can be achieved by introducing additional terminal ligands bound to metal clusters.[219] Fig. 8 shows the influence of ion and metal particle doping on H_2 adsorption. The addition of ions or nanoparticles often reduces the SSA of the hybrid, calling into question the reliability of using the BET area as an indicator of H_2 storage capacities in MOFs and MOF-derived materials. However, all samples show an increase in H_2 adsorption, especially at room temperature (25 °C). To improve H_2 storage, it is thus crucial to design novel MOF materials that not only have customized pore sizes and substantial void volumes, but also contain highly efficient adsorption sites. Among these sites are exposed metal ions, whose binding enthalpy lies between −20 and −30 kJ mol^{-1}.[161]

- **Metal ion doping of MOFs:** Metal ions can be introduced into the MOF matrix by ion exchange procedures as well as by chemical reduction methods, with the aim of increasing the adsorption enthalpy. Peedikakkal *et al.* showed that metal-exchanged MOF-5@Ni and MOF-5@Co exhibit slightly higher H_2 uptake (about 5 wt%) compared with the parent MOF-5.[90] Adsorption results by Prabhakaran and Deschamps revealed a substantial increase in the H_2 uptake capacity of MIL-101 thanks to the synergistic modification involving activated carbon and lithium doping (at both −196 °C and 25 °C). The H_2 storage capacity (−196 °C, 1 bar) of the doped MOF (MIL-101@AC-Li) showed an H_2 uptake of 1.60 wt% compared with 1.20 wt% in undoped MIL-101.[204] Prabhakaran *et al.* demonstrated that Li^+ doping (830 ppm) of MIL-101@SWCNTs improved H_2 uptake by more than twofold (4.96–10.43 mg g^{-1}) at 25 °C and 90 bar.[160]

- **Metal nanoparticles on MOFs:** The synthesis of MOF hybrids with metal nanoparticles involves incorporating the latter into the MOF structure using template methods or pre-synthesis strategies. This introduction effectively increases the number of adsorption sites, boosts adsorption enthalpy and enables synergistic physical–chemical H_2 adsorption. In particular, MOF@Pd hybrids have received considerable attention because Pd can absorb large amounts of H_2 at ambient temperature and pressure. Cheon *et al.* reported that H_2 sorption capacity was increased to 1.48 wt% at −196 °C and 1 atm, com-

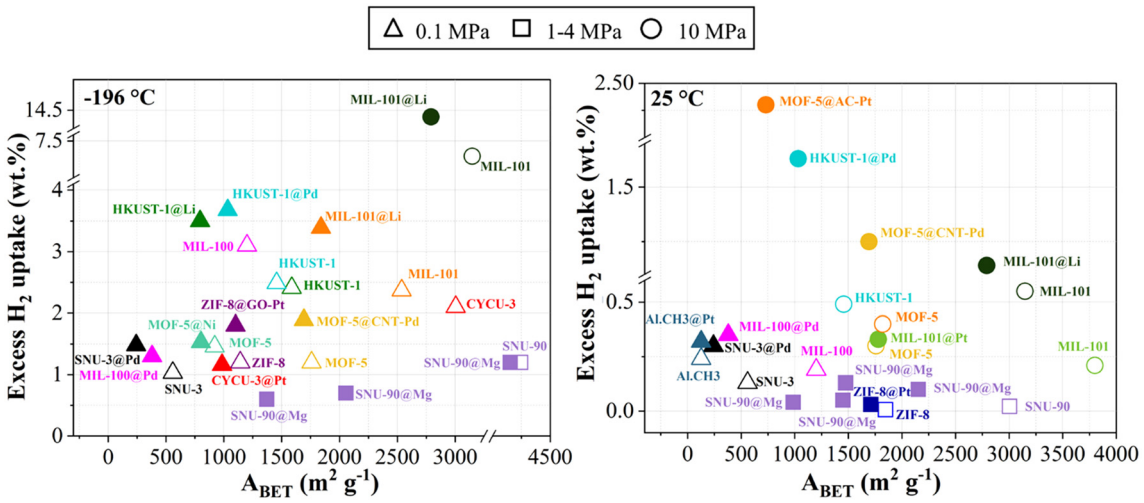

Fig. 8 Influence of adding metal particles into MOFs on the H_2 storage capacities of the resultant hybrid materials (○●ref. 204); (△▲, △▲ ref. 205); (△▲ ref. 206); (△▲, ○● ref. 207); (○●, △▲ ref. 90); (□■ ref. 208); (○●, △▲ ref. 209); (△▲ ref. 210); (△▲ ref. 162); (○● ref. 211); (□■ ref. 212); (△▲ ref. 213); (△▲ ref. 214).

pared to 1.03 wt% for pure SNU-3 MOF (despite a 43% decrease in the surface area).[162] Zlotea *et al.* showed that the MIL-100(Al)@Pd hybrid doubled H_2 uptake compared with the original MOF at room temperature.[206] Yang *et al.* loaded Pt into MOF-5@CNT hybrids to further increase H_2 storage capacity. The hybrid was prepared by *in situ* incorporation of the as-prepared Pt-loaded MWCNTs into MOF-5 crystals. Four materials were evaluated in terms of H_2 uptake: MWCNTs (A_{BET} = 147 m^2 g^{-1}), MWCNTs-Pt (A_{BET} = 124 m^2 g^{-1}), MOF-5 (A_{BET} = 1758 m^2 g^{-1}) and MOF@MWCNT-Pt (A_{BET} = 1692 m^2 g^{-1}). The authors studied H_2 uptake at −196 °C and 1 bar, as well as 25 °C and 100 bar. The highest H_2 uptake (−196 °C and 1 bar) was observed for MOF@MWCNT-Pt with 1.89 wt%, followed by MOF-5 with 1.20 wt%. At 25 °C and 100 bar, MOF@MWCNT-Pt showed much higher H_2 uptake values compared to the other materials, reaching 1.25 wt%.[207]

Prabhakaran and Deschamps synthesized a hybrid MOF by incorporating an AC, namely NORIT-RB3, during the synthesis of MIL-101, as well as lithium at different concentrations. H_2 adsorption capacities were evaluated at −196 °C and 25 °C, using pressures up to 100 bar. The highest H_2 uptakes were obtained for the MIL-101-B@AC-Li material, with 14.4 wt% at −196 °C and 1.1 wt% at 25 °C, both at 100 bars. Although the A_{BET} of the MIL-101-B@AC-Li material was much lower, 2791 m^2 g^{-1} than those of MIL-101, 3148 m^2 g^{-1}, and MIL-101@AC, 3458 m^2 g^{-1}, and slightly lower than that of MIL-101-A@AC-Li, 2958 m^2 g^{-1}, all of these hybrids provided H_2 uptake capacities >100 mg g^{-1} (10 wt%) at −196 °C. However, the significantly lower A_{BET} value of MIL-101-C@AC-Li (1868 m^2 g^{-1}) compromised higher H_2 uptakes, reaching a maximum of 87.70 mg g^{-1} at −196 °C.[204]

4.2.2. MOF hybrids with carbon materials for hydrogen storage. In this section, we examine how the addition of carbon materials improves the properties relevant to H_2 storage described in section 3.

- Increase in surface area: The addition of carbon-based materials to the MOF matrix often increases the SSA of the resulting MOF hybrid, enhancing its adsorption capacity at cryogenic and near-ambient temperatures.[199,204,220–222,226,227] Fig. 9 shows the effect of the BET area on H_2 adsorption for pure MOFs and for MOF hybrids with carbon-based materials at different storage pressures.

Yang *et al.* prepared MOF-5@MWCNT hybrids using acid-treated MWCNTs and MOF-5. The resultant materials exhibited a higher Langmuir specific surface area, from 2160 to 3550 m^2 g^{-1}, resulting in an approximately 50% increase in H_2 storage capacity at 25 °C and 95 bar (from 0.3 to 0.6 wt%) and a 25% increase in H_2 storage capacity at −196 °C and 1 bar (from 1.2 to 1.5 wt%). Furthermore, these hybrids demonstrated significantly improved stability in the presence of ambient moisture.[131] Petit *et al.* synthesized copper-based MOF@graphite oxide hybrids, and four materials were evaluated for H_2 adsorption: HKUST-1, HKUST-1@GO (5 wt%), HKUST-1@GO (9 wt%), and HKUST-1@GO (18 wt%). A_{BET} and H_2 uptake were 990 m^2 g^{-1} and 2.2 wt% for HKUST-1, 989 m^2 g^{-1} and 2.4 wt% for HKUST-1@GO (5 wt%), 1002 m^2 g^{-1} and 2.2 wt% for HKUST-1@GO (9 wt%), and 996 m^2 g^{-1} and 2.0 wt% for HKUST-1@GO (18 wt%), respectively. The authors attributed the improved uptake to the formation of new small pores for the hybrids.[221]

Prasanth *et al.* incorporated SWCNTs into MIL-101, and the best-performing material, incorporating 8 wt% of SWCNTs, presented H_2 sorption capacities of 9.2 wt% (at −196 °C and 6 MPa) and 0.6 wt% (at 25 °C and 6 MPa) compared with 6.4 wt% and 0.2 wt%, respectively, for the pristine MIL-101. Although this material has a slightly lower SSA, the authors ascribed these higher H_2 sorption capacities to the reduction in pore size and the increase in micropore volume in the hybrid due to the incorporation of SWCNTs.[218] Liu *et al.* hybridized Cu-MOFs with graphene oxide (GO) and achieved about

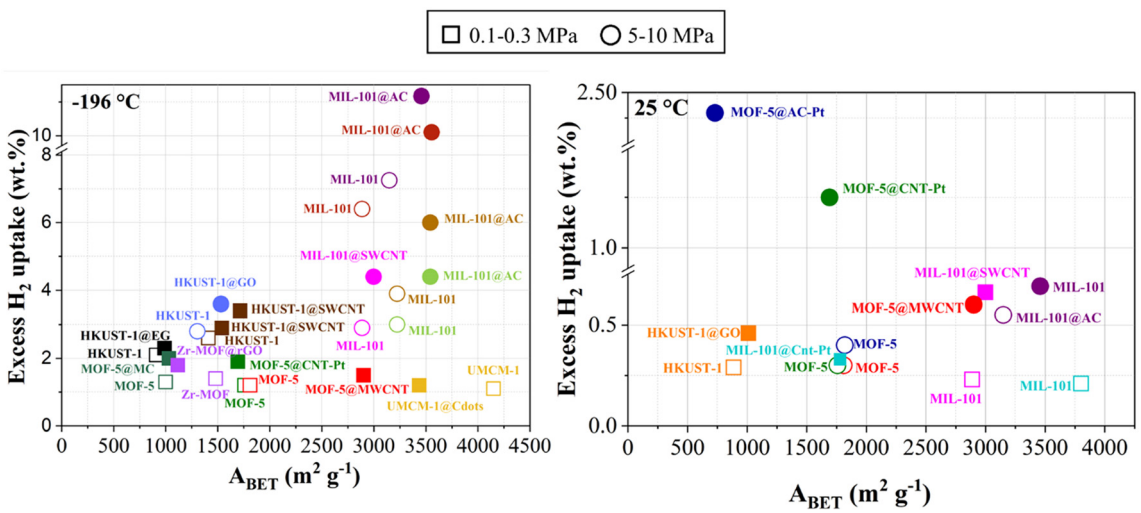

Fig. 9 Excess H_2 uptake of MOF hybrids reported in recent studies at −196 °C (left) and 25 °C (right) (○● ref. 220); (□■ ref. 221); (□■ ref. 222); (□■ ref. 223); (○●, □■ ref. 131); (□■, ○● ref. 207); (□■ ref. 175); (○● ref. 224); (□■ ref. 214); (○●, ○● ref. 158); (○●, □■ ref. 218); (○●, □■ ref. 159); (○● ref. 204); (□■ ref. 225).

30% higher H_2 capacities at −196 °C and 4.2 MPa due to the increased SSA.[220] Rallapalli *et al.* introduced activated carbon (AC) during the synthesis of MIL-101(Cr), and the best-performing material reached an A_{BET} of 3556 m^2 g^{-1} and an H_2 uptake of 10.1 wt% at −196 °C and 6 MPa, outperforming pristine MIL-101 (A_{BET} = 2887 m^2 g^{-1} and 6.4 wt% H_2 uptake under the same conditions[159]). Li *et al.* used carbon nanodots (CDs) to prepare UMCM-1@CD materials and the best H_2 uptake was 1.2 wt% at −196 °C and 0.1 MPa, slightly higher than that of UMCM-1 with 1.1 wt%. The authors suggested that the improvement was due to specific interactions between polar functional groups, *e.g.* –COOH and –OH, on the CD surface and H_2 molecules.[225] Yu *et al.* investigated MIL-101(Cr) and a MIL-101(Cr)@AC hybrid that displayed a maximum excess H_2 uptake (at −196 °C and 10 MPa) of 8.2 and 13.5 wt%, respectively, due to an increase in A_{BET} from 3407 for the pristine MOF to 3542 m^2 g^{-1} for the hybrid.[158]

The morphology, not just the texture, of the MOF hybrid often changes with the percentage of carbon-based material added. Fig. 10a and b show the HKUST-1@GO hybrid modified by increasing concentrations of GO from 1 to 2.5 g L^{-1}. The morphology of both samples changed significantly on reaching the highest GO concentration tested. In addition to the typical polyhedral crystals, distinctive rod- and flower-like structures appeared. Fig. 10c and d show the characteristic morphology of the Co-bpdc and Co-bpdc@MWCNT hybrids. In Fig. 10c, the Co-bpdc crystal exhibits a rectangular structure and Fig. 10d clearly shows the successful synthesis of a hybrid of MWCNTs with Co-bpdc.

Although GO had no measurable SSA by N_2 adsorption at −196 °C, the total SSA of the HKUST-1@GO hybrid remained constant or even increased with the addition of GO up to a GO concentration in solution of 2.5 g L^{-1} (see Fig. 10e).[228]

- **Increase in thermal stability**: The presence of a carbon-based material can also increase the thermal stability of the hybrid.[175,222] Policicchio *et al.* provided an overview of the thermal stability of hybrids obtained after the incorporation of nanographite (nGr) during the synthesis of UiO-66. In addition to a notable increase in material porosity (~30%), linker decomposition in all hybrids occurred at a temperature of around 80 °C higher than that of the pure MOF, probably due to changes in heat capacity caused by the introduction of nGr.[9]

Jiang *et al.* studied the influence of introducing MWCNTs into the MOF-5 matrix, obtaining a hybrid that showed a 6% increase in thermal stability.[175] Rojas-Garcia *et al.* showed that HKUST-1@SWCNT materials exhibit improved thermal stability (320 °C) compared to pristine HKUST-1 (220 °C) using an InVia Renishaw Raman instrument equipped with a Linkam cell.[222]

- **Increase in hydrophobicity**: Kim *et al.* used carbon black to fabricate a hybrid with MOF-5 and demonstrated that it did not affect the integrity of the MOF-5 and effectively protected the framework from moisture.[230] For the same MOF, Yang and Park reported that an amorphous carbon-coated MOF-5 could be prepared by a simple thermal modification process carried out under an N_2 atmosphere in a temperature range of 480–530 °C. Amorphous carbon-coated MOF-5 samples were found to have reduced BET areas (1740 *vs.* 3450 m^2 g^{-1}), but displayed better water stability compared with pristine MOF-5.[231] Jayaramulu *et al.* obtained a hybrid material using a highly fluorinated graphene oxide (HFG) and ZIF-8 (ZIF-8@HFG). The material exhibited superhydrophobic behavior with an exceptionally high water contact angle of 162°.[232]

- **Increase in thermal conductivity**: The addition of carbon-based materials to a MOF boosts its thermal conductivity, making it more efficient at conducting and dissipating heat. The degree of improvement depends on factors such as the filler type, concentration and dispersion. Nandasiri *et al.* reported an ~23% improvement in thermal conductivity by adding GO to the MOF matrix MIL-101(Cr).[233] The addition of 10 wt% expanded natural graphite to MOF-5 pellets with a density of 0.5 g cm^{-3} was previously found to improve thermal conduction near room temperature by a factor of 5 (compared with undoped MOF-5 pellets).[234] A similar behavior was observed by Farrando-Pérez *et al.* for the HKUST-1@graphite flake hybrid, showing that the thermal conductivity of the hybrid monolith (50 wt% graphite flakes) was 3.15 W m^{-1} K^{-1} *vs.* 0.49 W m^{-1} K^{-1} for the pure HKUST-1 monolith. In terms of H_2 uptake, the hybrid monolith with 10 wt% graphite flakes showed the best result with 1.7 wt% *vs.* 1.25 wt% for the pure HKUST-1 monolith.[143]

4.2.3. MOF hybrids with other inorganic materials. Hybrids with MOFs have been used for various applications, such as CO_2 capture, and can include alternative materials such as zeolites, cellulose and clays.[235] MOFs@clay hybrids include feedstock materials such as attapulgite, amino-clay, cordierite, kaolin and bentonite. Wang *et al.* studied the influence of introducing diatomite (Da) into the MIL-101 (Cr) matrix. Their study evaluated the H_2 storage capacity of the Cr-MOF@Da hybrid at 25 °C and 1 bar. The H_2 adsorption isotherms showed a linear increase as the wt% of diatomite increased, obtaining 0.022 wt% for Cr-MIL-101@Da-4. The hybrids also showed improved thermal stability.[236]

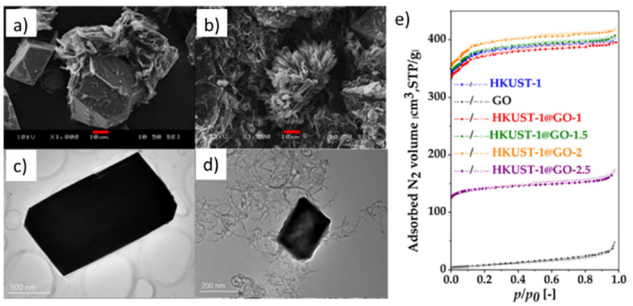

Fig. 10 (a) SEM images of HKUST-1@1g L^{-1} GO; (b) SEM images of HKUST-1@2.5 g L^{-1} GO. Scale bar is 10 μm (reproduced from ref. 228 © 1996–2024 MDPI); (c) TEM images of Co-bpdc (cobalt benzene-1,4-dicarboxylate) as a pure MOF; (d) TEM images of Co-bpdc@MWCNTs as a hybrid (reproduced from ref. 229 © 1996–2024 MDPI); (e) N_2 adsorption–desorption isotherms (–196 °C) of pristine GO, HKUST-1 and hybrid materials with different GO contents (reproduced from ref. 228 © 1996–2024 MDPI).

MOF@clays have been the subject of research interest, especially for the development of complex geometries of MOFs using 3D printing.[237] MOFs@zeolite hybrids combine the high SSA of MOFs with the high mechanical strength of zeolites. By selecting the type of synthesis, a core–shell structure can be obtained that may offer certain advantages, such as gas separation, hydrophobicity, *etc*.[238] For instance, Musyoka *et al.* fabricated a MIL-101(Cr)@zeolite-templated carbon (ZTC) hybrid for H_2 storage applications. H_2 adsorption measurements were carried out at −196 °C up to 1 bar. The hybrid material was compared with the individual materials and showed an increased surface area and H_2 uptake capacity of 2957 m^2 g^{-1} and 2.55 wt%, respectively. These results are significantly better than those obtained with MIL-101 (2552 m g^{-1}, 2.39 wt%) and ZTC (2577 m^2 g^{-1}, 2.39 wt%).[239]

5. Conclusions

The development of MOF-based hybrid adsorbents, combining MOFs with a variety of other materials and nanostructures, has attracted considerable interest in recent times. This approach aims to improve the performance and scalability of MOFs, opening up possibilities for future materials.

MOFs alone, due to their versatile structures, high surface areas and substantial pore volumes, are already considered promising materials for H_2 storage, as evidenced by NU100, which reaches 9.05 wt% at 7 MPa and −196 °C. Moreover, a variety of synthesis methods enables the nanopore structure of MOFs to be controlled, which is essential for their applicability in adsorption. Our review covered different synthesis techniques, delineating their respective advantages and drawbacks in controlling MOF parameters, as well as characterizing MOFs and their hybrids. By recognizing the potential of MOFs, increasing the SSA and optimizing pore size distribution should make it possible to increase H_2 storage capacities in line with the DOE specifications.

To optimize hydrogen storage under ambient conditions, strategies such as linker functionalization and the introduction of unsaturated metal centers are highly effective. A notable example is that of exposed metal ions, which often have binding enthalpies ranging from −20 to −30 kJ mol^{-1}. Other advances concern the creation of competitive MOF hybrids, especially through the incorporation of carbon materials, which show promise in increasing adsorption capacity, improving thermal stability and enhancing thermal conductivity. To improve the selectivity and stability of MOFs, MOF@MOF hybrids offer a promising approach. By integrating the characteristics of two distinct MOFs into a single, unified material, this method effectively combines their advantages. Combinations such as MOF@carbon-based materials preserve the advantages of MOFs while improving thermal conductivity, surface area and ease of shaping.

In conclusion, MOF-based hybrids represent a promising approach for improving H_2 storage capabilities, offering significant potential to meet the demanding standards set by the US DOE. Key areas of future research should focus on increasing the volumetric capacity of these materials, as their gravimetric performance is already outstanding, but volumetric improvements are essential for practical applications such as transportation and portable energy systems. These developments will play a decisive role in optimizing the performance of MOF hybrids and advancing their viability for commercial hydrogen storage applications.

Abbreviation

$(-\Delta H)_{ads}$	Adsorption enthalpy
A_{BET}	Brunauer–Emmett–Teller area
BDC	1,4-Benzenedicarboxylic acid
BET	Brunauer–Emmett–Teller
BPDC	Biphenyldicarboxylate
BTC	Benzene-1,3,5-Tricarboxylic acid
CDs	Carbon dots
Co-bpdc	Cobalt benzene-1,4-dicarboxylate
COFs	Covalent organic frameworks
DMF	*N*,*N*-Dimethylformamide
DOE	U.S. Department of Energy
FTIR	Fourier transform infrared spectroscopy
GL	Graphene-like
GO	Graphene oxide
H_2	Hydrogen
ILs	Ionic liquids
IMOFs	Interpenetrated MOFs
MIL	Materials of Institut Lavoiser
MOFs	Metal organic frameworks
MWCNTs	Multi-walled carbon nanotubes
nGr	Nano graphite
NMR	Nuclear magnetic resonance
NU	Northewestern University
PBUs	Primary building units
PCPs	Porous coordination polymers
PDC	3,5-Pyridine dicarboxylic acid
PSD	Pore size distribution
PTFE	Polytetrafluoroethylene
QDs	Quantum dots
RAM	Resonant acoustic mixing
SBUs	Secondary building units
SEM	Scanning electron microscopy
SSA	Specific surface area
SWCNT	Single-walled carbon nanotubes
TGA	Thermogravimetric analysis
UIO	Universitetet i Oslo
XRD	X-ray diffraction analysis
ZTC	Zeolite-templated carbon

Author contributions

L.J.-L.: writing – original draft and formal analysis; R.M.-O.: review & editing, formal analysis, and supervision; L.G. A.:

writing – original draft and formal analysis; A.C.: review & editing and supervision; V.F. review & editing, supervision, project administration, and formal analysis.

Data availability

The data supporting this article have been included as part of the ESI.†

No primary research results, software or code have been included and no new data were generated or analysed as part of this review.

Conflicts of interest

There are no conflicts to declare.

Acknowledgements

This work was made possible thanks to (i) the SOLHYD project (ANR-22-PEHY-0007) funded by the Agence Nationale de la Recherche, (ii) the FRCR HyPE project funded by Région Grand-Est, and (iii) TALiSMAN and TALiSMAN2 projects funded by FEDER. De Araujo, L. G. acknowledges the MOPGA program, funded by the French Ministry of Europe and Foreign Affairs, in collaboration with the French Ministry of Higher Education and Research.

References

1 E. Ilisca, Microporous Materials for Hydrogen Liquefiers and Storage Vessels, *J. Mater. Sci. Lett.*, 2022, **3**, 1–10.
2 M. Ball and M. Wietschel, *The Hydrogen Economy: Opportunities and Challenges*, Cambridge University Press, 2009, pp. 671.
3 D. J. Durbin and C. Malardier-Jugroot, Review of hydrogen storage techniques for on board vehicle applications, *Int. J. Hydrogen Energy*, 2013, **38**(34), 14595–14617.
4 S. Evro, B. A. Oni and O. S. Tomomewo, Carbon neutrality and hydrogen energy systems, *Int. J. Hydrogen Energy*, 2024, **78**, 1449–1467.
5 G. Squadrito, G. Maggio and A. Nicita, The green hydrogen revolution, *Renewable Energy*, 2023, **216**, 119041.
6 R. Morales-Ospino, L. Jiménez-López, A. Celzard and V. Fierro, Hydrogen – Storage | Physical storage, in *Reference Module in Chemistry, Molecular Sciences and Chemical Engineering [Internet]*, Elsevier, 2024. Available from: **https://www.sciencedirect.com/science/article/pii/B9780323960229002905** [cited 2024 Jun 27].
7 S. Bordiga, L. Regli, F. Bonino, E. Groppo, C. Lamberti, B. Xiao, *et al.*, Adsorption properties of HKUST-1 toward hydrogen and other small molecules monitored by IR, *Phys. Chem. Chem. Phys.*, 2007, **9**(21), 2676–2685.
8 O. K. Farha, A. Özgür Yazaydın, I. Eryazici, C. D. Malliakas, B. G. Hauser, M. G. Kanatzidis, *et al.*, De novo synthesis of a metal–organic framework material featuring ultrahigh surface area and gas storage capacities, *Nat. Chem.*, 2010, **2**(11), 944–948.
9 A. Policicchio, M. Florent, A. Celzard, V. Fierro, J. Jagiello and T. J. Bandosz, Enhancing the gas adsorption capacities of UiO-66 by nanographite addition, *Microporous Mesoporous Mater.*, 2020, **309**, 110571.
10 M. Hasanzadeh, A. Simchi and H. Shahriyari Far, Nanoporous composites of activated carbon-metal organic frameworks for organic dye adsorption: Synthesis, adsorption mechanism and kinetics studies, *J. Ind. Eng. Chem.*, 2020, **81**, 405–414.
11 C. Liu, J. Wang, J. Wan and C. Yu, MOF-on-MOF hybrids: Synthesis and applications, *Coord. Chem. Rev.*, 2021, **432**, 213743.
12 M. Jouyandeh, F. Tikhani, M. Shabanian, F. Movahedi, S. Moghari, V. Akbari, *et al.* Synthesis, characterization, and high potential of 3D metal–organic framework (MOF) nanoparticles for curing with epoxy, *J. Alloys Compd.*, 2020, **829**, 154547.
13 A. Schoedel and S. Rajeh, Why Design Matters: From Decorated Metal Oxide Clusters to Functional Metal–Organic Frameworks, *Top. Curr. Chem.*, 2020, **378**(1), 19.
14 X. W. Liu, T. J. Sun, J. L. Hu and S. D. Wang, Composites of metal–organic frameworks and carbon-based materials: preparations, functionalities and applications, *J. Mater. Chem. A*, 2016, **4**(10), 3584–3616.
15 F. A. A. Paz, J. Klinowski, S. M. F. Vilela, J. P. C. Tomé, J. A. S. Cavaleiro and J. Rocha, Ligand design for functional metal–organic frameworks, *Chem. Soc. Rev.*, 2012, **41**(3), 1088–1110.
16 S. Soni, P. Bajpai and C. Arora, A review on metal-organic framework: synthesis, properties and application, *Charact. Appl. Nanomater.*, 2018, **2**, 87–106.
17 S. Kitagawa, R. Kitaura and S. I. Noro, Functional Porous Coordination Polymers, *Angew. Chem., Int. Ed.*, 2004, **43**(18), 2334–2375.
18 P. Rocío-Bautista, I. Taima-Mancera, J. Pasán and V. Pino, Metal-Organic Frameworks in Green Analytical Chemistry, *Separations*, 2019, **6**(3), 33.
19 S. P. Shet, S. Shanmuga Priya, K. Sudhakar and M. Tahir, A review on current trends in potential use of metal-organic framework for hydrogen storage, *Int. J. Hydrogen Energy*, 2021, **46**(21), 11782–11803.
20 J. L. C. Rowsell and O. M. Yaghi, Metal–organic frameworks: a new class of porous materials, *Microporous Mesoporous Mater.*, 2004, **73**(1), 3–14.
21 N. Stock and S. Biswas, Synthesis of Metal-Organic Frameworks (MOFs): Routes to Various MOF Topologies, Morphologies, and Composites, *Chem. Rev.*, 2012, **112**(2), 933–969.
22 D. Sud and G. Kaur, A comprehensive review on synthetic approaches for metal-organic frameworks: From tra-

ditional solvothermal to greener protocols, *Polyhedron*, 2021, **193**, 114897.
23 Z. Zheng, H. L. Nguyen, N. Hanikel, K. K. Y. Li, Z. Zhou, T. Ma, *et al.*, High-yield, green and scalable methods for producing MOF-303 for water harvesting from desert air, *Nat. Protoc.*, 2023, **18**(1), 136–156.
24 D. J. Tranchemontagne, J. R. Hunt and O. M. Yaghi, Room temperature synthesis of metal-organic frameworks: MOF-5, MOF-74, MOF-177, MOF-199, and IRMOF-0, *Tetrahedron*, 2008, **64**(36), 8553–8557.
25 M. Sánchez-Sánchez, N. Getachew, K. Díaz, M. Díaz-García and Y. Chebude, Díaz I. Synthesis of metal–organic frameworks in water at room temperature: salts as linker sources, *Green Chem.*, 2015, **17**(3), 1500–1509.
26 N. Getachew, Y. Chebude, I. Diaz and M. Sanchez-Sanchez, Room temperature synthesis of metal organic framework MOF-2, *J. Porous Mater.*, 2014, **21**(5), 769–773.
27 S. Proch, J. Herrmannsdörfer, R. Kempe, C. Kern, A. Jess, L. Seyfarth, *et al.*, Pt@MOF-177: Synthesis, Room-Temperature Hydrogen Storage and Oxidation Catalysis, *Chem. – Eur. J.*, 2008, **14**(27), 8204–8212.
28 M. Ebrahimi and M. Mansournia, Rapid room temperature synthesis of zeolitic imidazolate framework-7 (ZIF-7) microcrystals, *Mater. Lett.*, 2017, **189**, 243–247.
29 E. Biemmi, S. Christian, N. Stock and T. Bein, High-throughput screening of synthesis parameters in the formation of the metal-organic frameworks MOF-5 and HKUST-1, *Microporous Mesoporous Mater.*, 2009, **117**(1), 111–117.
30 W. W. Lestari, M. Adreane, C. Purnawan, H. Fansuri, N. Widiastuti and S. B. Rahardjo, Solvothermal and electrochemical synthetic method of HKUST-1 and its methane storage capacity, *IOP Conf. Ser.:Mater. Sci. Eng.*, 2016, **107**(1), 012030.
31 N. Pokhrel, P. K. Vabbina and N. Pala, Sonochemistry: Science and Engineering, *Ultrason. Sonochem.*, 2016, **29**, 104–128.
32 S. Głowniak, B. Szczęśniak, J. Choma and M. Jaroniec, Recent Developments in Sonochemical Synthesis of Nanoporous Materials, *Molecules*, 2023, **28**(6), 2639.
33 L. G. Qiu, Z. Q. Li, Y. Wu, W. Wang, T. Xu and X. Jiang, Facile synthesis of nanocrystals of a microporous metal–organic framework by an ultrasonic method and selective sensing of organoamines, *Chem. Commun.*, 2008, (31), 3642–3644.
34 C. Vaitsis, G. Sourkouni and C. Argirusis, Metal Organic Frameworks (MOFs) and ultrasound: A review, *Ultrason. Sonochem.*, 2019, **52**, 106–119.
35 H. M. Yang, X. Liu, X. L. Song, T. L. Yang, Z. H. Liang and C. M. Fan, In situ electrochemical synthesis of MOF-5 and its application in improving photocatalytic activity of BiOBr, *Trans. Nonferrous Met. Soc. China*, 2015, **25**(12), 3987–3994.
36 S. Kalhor, M. Zarei, M. A. Zolfigol, H. Sepehrmansourie, D. Nematollahi, S. Alizadeh, *et al.* Anodic electrosynthesis of MIL-53(Al)-N($CH_2PO_3H_2$)$_2$ as a mesoporous catalyst for synthesis of novel (N-methyl-pyrrol)-pyrazolo[3,4-b]pyridines via a cooperative vinylogous anomeric based oxidation, *Sci. Rep.*, 2021, **11**(1), 19370.
37 A. Martinez Joaristi, J. Juan-Alcañiz, P. Serra-Crespo, F. Kapteijn and J. Gascon, Electrochemical Synthesis of Some Archetypical Zn^{2+}, Cu^{2+}, and Al^{3+} Metal Organic Frameworks, *Cryst. Growth Des.*, 2012, **12**(7), 3489–3498.
38 S. Yadnum, J. Roche, E. Lebraud, P. Négrier, P. Garrigue, D. Bradshaw, *et al.*, Site-Selective Synthesis of Janus-type Metal-Organic Framework Composites, *Angew. Chem., Int. Ed.*, 2014, **53**(15), 4001–4005.
39 V. Vm and G. Nageswaran, Review—Direct Electrochemical Synthesis of Metal Organic Frameworks, *J. Electrochem. Soc.*, 2020, **167**(15), 155527.
40 A. M. Antonio, J. Rosenthal and E. D. Bloch, Electrochemically Mediated Syntheses of Titanium(III)-Based Metal–Organic Frameworks, *J. Am. Chem. Soc.*, 2019, **141**(29), 11383–11387.
41 M. Hartmann, S. Kunz, D. Himsl, O. Tangermann, S. Ernst and A. Wagener, Adsorptive Separation of Isobutene and Isobutane on $Cu_3(BTC)_2$, *Langmuir*, 2008, **24**(16), 8634–8642.
42 P. Kunal and T. J. Toops, A Review of Microwave-Assisted Synthesis-Based Approaches to Reduce Pd-Content in Catalysts, *Catalysts*, 2020, **10**(9), 991.
43 G. A. Tompsett, W. C. Conner and K. S. Yngvesson, Microwave Synthesis of Nanoporous Materials, *ChemPhysChem*, 2006, **7**(2), 296–319.
44 Z. Ni and R. I. Masel, Rapid Production of Metal–Organic Frameworks via Microwave-Assisted Solvothermal Synthesis, *J. Am. Chem. Soc.*, 2006, **128**(38), 12394–12395.
45 J. Klinowski, F. A. A. Paz, P. Silva and J. Rocha, Microwave-Assisted Synthesis of Metal–Organic Frameworks, *Dalton Trans.*, 2010, **40**(2), 321–330.
46 Z. Ni and R. I. Masel, Rapid Production of Metal–Organic Frameworks via Microwave-Assisted Solvothermal Synthesis, *J. Am. Chem. Soc.*, 2006, **128**(38), 12394–12395.
47 M. Taddei, P. V. Dau, S. M. Cohen, M. Ranocchiari, J. A. van Bokhoven, F. Costantino, *et al.*, Efficient microwave assisted synthesis of metal–organic framework UiO-66: optimization and scale up, *Dalton Trans.*, 2015, **44**(31), 14019–14026.
48 X. Wu, W. Xu, Z. Wang, H. Li, M. Wang, D. Zhang, *et al.*, Rapid microwave synthesis of Ru-supported partially carbonized conductive metal–organic framework for efficient hydrogen evolution, *Chem. Eng. J.*, 2022, **431**, 133247.
49 S. Wan, O. Xu and X. Zhu, Synthesis of ionic liquid modified metal-organic framework composites and its application in solid-phase extraction: a review, *Ionics*, 2021, **27**(2), 445–456.
50 T. P. Vaid, S. P. Kelley and R. D. Rogers, Structure-directing effects of ionic liquids in the ionothermal synthesis of metal–organic frameworks, *IUCrJ*, 2017, **4**(4), 380–392.
51 L. Peng, J. Zhang, J. Li, B. Han, Z. Xue and G. Yang, Surfactant-directed assembly of mesoporous metal–

organic framework nanoplates in ionic liquids, *Chem. Commun.*, 2012, **48**(69), 8688–8690.

52 C. Liu, G. Zhang, C. Zhao, X. Li, M. Li and H. Na, MOFs synthesized by the ionothermal method addressing the leaching problem of IL–polymer composite membranes, *Chem. Commun.*, 2014, **50**(91), 14121–14124.

53 M. Leonardi, M. Villacampa and J. Carlos Menéndez, Multicomponent mechanochemical synthesis, *Chem. Sci.*, 2018, **9**(8), 2042–2064.

54 B. Szczęśniak, S. Borysiuk, J. Choma and M. Jaroniec, Mechanochemical synthesis of highly porous materials, *Mater. Horiz.*, 2020, **7**(6), 1457–1473.

55 M. Afkhami-Ardekani, M. R. Naimi-Jamal, S. Doaee and S. Rostamnia, Solvent-Free Mechanochemical Preparation of Metal-Organic Framework ZIF-67 Impregnated by Pt Nanoparticles for Water Purification, *Catalysts*, 2023, **13**(1), 9.

56 D. Chen, J. Zhao, P. Zhang and S. Dai, Mechanochemical synthesis of metal–organic frameworks, *Polyhedron*, 2019, **162**, 59–64.

57 S. Tanaka, Chapter 10 – Mechanochemical synthesis of MOFs, in *Metal-Organic Frameworks for Biomedical Applications [Internet]*, ed. M. Mozafari, Woodhead Publishing, 2020. pp. 197–222. Available from: **https://www.sciencedirect.com/science/article/pii/B9780128169841000123** [cited 2023 Aug 29].

58 C. A. Tao and J. F. Wang, Synthesis of Metal Organic Frameworks by Ball-Milling, *Crystals*, 2021, **11**(1), 15.

59 H. M. Titi, J. L. Do, A. J. Howarth, K. Nagapudi and T. Friščić, Simple, scalable mechanosynthesis of metal–organic frameworks using liquid-assisted resonant acoustic mixing (LA-RAM), *Chem. Sci.*, 2020, **11**(29), 7578–7584.

60 R. Seetharaj, P. V. Vandana, P. Arya and S. Mathew, Dependence of solvents, pH, molar ratio and temperature in tuning metal organic framework architecture, *Arabian J. Chem.*, 2019, **12**(3), 295–315.

61 A. A. Yakovenko, Z. Wei, M. Wriedt, J. R. Li, G. J. Halder and H. C. Zhou, Study of Guest Molecules in Metal–Organic Frameworks by Powder X-ray Diffraction: Analysis of Difference Envelope Density, *Cryst. Growth Des.*, 2014, **14**(11), 5397–5407.

62 D. Banerjee, J. Finkelstein, A. Smirnov, P. M. Forster, L. A. Borkowski, S. J. Teat, *et al.*, Synthesis and Structural Characterization of Magnesium Based Coordination Networks in Different Solvents, *Cryst. Growth Des.*, 2011, **11**(6), 2572–2579.

63 T. A. Mulyati, R. Ediati and A. Rosyidah, Influence of Solvothermal Temperatures and Times on Crystallinity and Morphology of MOF-5, *Indones. J. Chem.*, 2015, **15**(2), 101–107.

64 B. Li, Y. Zhang, D. Ma, L. Li, G. Li, G. Li, *et al.*, A strategy toward constructing a bifunctionalized MOF catalyst: post-synthetic modification of MOFs on organic ligands and coordinatively unsaturated metal sites, *Chem. Commun.*, 2012, **48**(49), 6151–6153.

65 S. Ko, F. Gao, X. Yao, H. Yi, X. Tang, C. Wang, *et al.*, Synthesis of metal–organic frameworks (MOFs) and their application in the selective catalytic reduction of NOx with NH_3, *New J. Chem.*, 2022, **46**(33), 15758–15775.

66 C. Mottillo and T. Friščić, Advances in Solid-State Transformations of Coordination Bonds: From the Ball Mill to the Aging Chamber, *Molecules*, 2017, **22**(1), 144.

67 H. Luo, F. Cheng, L. Huelsenbeck and N. Smith, Comparison between conventional solvothermal and aqueous solution-based production of UiO-66-NH_2: Life cycle assessment, techno-economic assessment, and implications for CO_2 capture and storage, *J. Environ. Chem. Eng.*, 2021, **9**(2), 105159.

68 S. Dai, C. Simms, I. Dovgaliuk, G. Patriarche, A. Tissot, T. N. Parac-Vogt, *et al.*, Monodispersed MOF-808 Nanocrystals Synthesized via a Scalable Room-Temperature Approach for Efficient Heterogeneous Peptide Bond Hydrolysis, *Chem. Mater.*, 2021, **33**(17), 7057–7066.

69 M. Díaz-García, Á. Mayoral, I. Díaz and M. Sánchez-Sánchez, Nanoscaled M-MOF-74 Materials Prepared at Room Temperature, *Cryst. Growth Des.*, 2014, **14**(5), 2479–2487.

70 S. He, L. Wu, X. Li, H. Sun, T. Xiong, J. Liu, *et al.*, Metal-organic frameworks for advanced drug delivery, *Acta Pharm. Sin. B*, 2021, **11**(8), 2362–2395.

71 D. W. Jung, D. A. Yang, J. Kim, J. Kim and W. S. Ahn, Facile synthesis of MOF-177 by a sonochemical method using 1-methyl-2-pyrrolidinone as a solvent, *Dalton Trans.*, 2010, **39**(11), 2883–2887.

72 W. J. Son, J. Kim, J. Kim and W. S. Ahn, Sonochemical synthesis of MOF-5, *Chem. Commun.*, 2008, (47), 6336–6338.

73 W. Xu, G. Li, W. Li and H. Zhang, Facile room temperature synthesis of metal–organic frameworks from newly synthesized copper/zinc hydroxide and their application in adsorptive desulfurization, *RSC Adv.*, 2016, **6**(44), 37530–37534.

74 J. H. Lee, Y. Ahn and S. Y. Kwak, Facile Sonochemical Synthesis of Flexible Fe-Based Metal–Organic Frameworks and Their Efficient Removal of Organic Contaminants from Aqueous Solutions, *ACS Omega*, 2022, **7**(27), 23213–23222.

75 H. Ren and T. Wei, Electrochemical Synthesis Methods of Metal-Organic Frameworks and Their Environmental Analysis Applications: A Review, *ChemElectroChem*, 2022, **9**(13), e202200196.

76 H. Al-Kutubi, J. Gascon, E. J. R. Sudhölter and L. Rassaei, Electrosynthesis of Metal–Organic Frameworks: Challenges and Opportunities, *ChemElectroChem*, 2015, **2**(4), 462–474.

77 W. Wu, G. E. Decker, A. E. Weaver, A. I. Arnoff, E. D. Bloch and J. Rosenthal, Facile and Rapid Room-Temperature Electrosynthesis and Controlled Surface Growth of Fe-MIL-101 and Fe-MIL-101-NH_2, *ACS Cent. Sci.*, 2021, **7**(8), 1427–1433.

78 Y. R. Lee, J. Kim and W. S. Ahn, Synthesis of metal-organic frameworks: A mini review, *Korean J. Chem. Eng.*, 2013, **30**(9), 1667–1680.

79 S. H. Jhung, J. H. Lee, P. M. Forster, G. Férey, A. K. Cheetham and J. S. Chang, Microwave Synthesis of Hybrid Inorganic–Organic Porous Materials: Phase-Selective and Rapid Crystallization, *Chem. – Eur. J.*, 2006, **12**(30), 7899–7905.

80 H. K. Liu, T. H. Tsao, Y. T. Zhang and C. H. Lin, Microwave synthesis and single-crystal-to-single-crystal transformation of magnesium coordination polymers exhibiting selective gas adsorption and luminescence properties, *CrystEngComm*, 2009, **11**(7), 1462–1468.

81 T. J. Azbell, T. A. Pitt, M. M. Bollmeyer, C. Cong, K. M. Lancaster and P. J. Milner, Ionothermal Synthesis of Metal-Organic Frameworks Using Low-Melting Metal Salt Precursors, *Angew. Chem., Int. Ed.*, 2023, **62**(17), e202218252.

82 P. Li, F. F. Cheng, W. W. Xiong and Q. Zhang, New synthetic strategies to prepare metal–organic frameworks, *Inorg. Chem. Front.*, 2018, **5**(11), 2693–2708.

83 R. E. Morris, Ionothermal synthesis—ionic liquids as functional solvents in the preparation of crystalline materials, *Chem. Commun.*, 2009, (21), 2990–2998.

84 S. Tanaka, K. Kida, T. Nagaoka, T. Ota and Y. Miyake, Mechanochemical dry conversion of zinc oxide to zeolitic imidazolate framework, *Chem. Commun.*, 2013, **49**(72), 7884–7886.

85 S. Głowniak, B. Szczęśniak, J. Choma and M. Jaroniec, Mechanochemistry: Toward green synthesis of metal–organic frameworks, *Mater. Today*, 2021, **46**, 109–124.

86 A. Pichon, A. Lazuen-Garay and S. L. James, Solvent-free synthesis of a microporous metal–organic framework, *CrystEngComm*, 2006, **8**(3), 211–214.

87 J. Xu, J. Liu, Z. Li, X. Wang, Y. Xu, S. Chen, *et al.*, Optimized synthesis of Zr(IV) metal organic frameworks (MOFs-808) for efficient hydrogen storage, *New J. Chem.*, 2019, **43**(10), 4092–4099.

88 K. Suresh, D. Aulakh, J. Purewal, D. J. Siegel, M. Veenstra and A. J. Matzger, Optimizing Hydrogen Storage in MOFs through Engineering of Crystal Morphology and Control of Crystal Size, *J. Am. Chem. Soc.*, 2021, **143**(28), 10727–10734.

89 X. Yang, T. Song, T. Su, J. Hu and S. Wu, Exploring the Influence of the Reused Methanol Solution for the Structure and Properties of the Synthesized ZIF-8, *Processes*, 2022, **10**(9), 1705.

90 A. M. P. Peedikakkal and I. H. Aljundi, Upgrading the Hydrogen Storage of MOF-5 by Post-Synthetic Exchange with Divalent Metal Ions, *Appl. Sci.*, 2021, **11**(24), 11687.

91 M. Usman, M. Y. Khan, T. Anjum, A. L. Khan, B. Hoque, A. Helal, *et al.*, Controlled Covalent Functionalization of ZIF-90 for Selective CO_2 Capture & Separation, *Membranes*, 2022, **12**(11), 1055.

92 Y. Liu, C. Wang, S. Ju, M. Li, A. Yuan and G. Zhu, FeCo-based hybrid MOF derived active species for effective oxygen evolution, *Prog. Nat. Sci.:Mater. Int.*, 2020, **30**(2), 185–191.

93 R. Ameloot, F. Vermoortele, J. Hofkens, F. C. De Schryver, D. E. De Vos and M. B. J. Roeffaers, Three-Dimensional Visualization of Defects Formed during the Synthesis of Metal–Organic Frameworks: A Fluorescence Microscopy Study, *Angew. Chem., Int. Ed.*, 2013, **52**(1), 401–405.

94 J. Schaber, S. Krause, S. Paasch, I. Senkovska, V. Bon, D. M. Többens, *et al.*, In Situ Monitoring of Unique Switching Transitions in the Pressure-Amplifying Flexible Framework Material DUT-49 by High-Pressure 129Xe NMR Spectroscopy, *J. Phys. Chem. C*, 2017, **121**(9), 5195–5200.

95 B. Chen, X. Zhao, A. Putkham, K. Hong, E. B. Lobkovsky, E. J. Hurtado, *et al.*, Surface Interactions and Quantum Kinetic Molecular Sieving for H_2 and D_2 Adsorption on a Mixed Metal–Organic Framework Material, *J. Am. Chem. Soc.*, 2008, **130**(20), 6411–6423.

96 J. L. Belof, A. C. Stern, M. Eddaoudi and B. Space, On the Mechanism of Hydrogen Storage in a Metal–Organic Framework Material, *J. Am. Chem. Soc.*, 2007, **129**(49), 15202–15210.

97 G. Sdanghi, R. L. S. Canevesi, A. Celzard, M. Thommes and V. Fierro, Characterization of Carbon Materials for Hydrogen Storage and Compression, *C*, 2020, **6**(3), 46.

98 T. He, P. Pachfule, H. Wu, Q. Xu and P. Chen, Hydrogen carriers, *Nat. Rev. Mater.*, 2016, **1**(12), 1–17.

99 D. A. Gómez-Gualdrón, P. Z. Moghadam, J. T. Hupp, O. K. Farha and R. Q. Snurr, Application of Consistency Criteria To Calculate BET Areas of Micro- And Mesoporous Metal–Organic Frameworks, *J. Am. Chem. Soc.*, 2016, **138**(1), 215–224.

100 R. Balderas-Xicohténcatl, P. Schmieder, D. Denysenko, D. Volkmer and M. Hirscher, High Volumetric Hydrogen Storage Capacity using Interpenetrated Metal–Organic Frameworks, *Energy Technol.*, 2018, **6**(3), 510–512.

101 R. Balderas-Xicohténcatl, M. Schlichtenmayer and M. Hirscher, Volumetric Hydrogen Storage Capacity in Metal–Organic Frameworks, *Energy Technol.*, 2018, **6**(3), 578–582.

102 M. Hirscher, Hydrogen Storage by Cryoadsorption in Ultrahigh-Porosity Metal–Organic Frameworks, *Angew. Chem., Int. Ed.*, 2011, **50**(3), 581–582.

103 M. Thommes, K. Kaneko, A. V. Neimark, J. P. Olivier, F. Rodriguez-Reinoso, J. Rouquerol, *et al.*, Physisorption of gases, with special reference to the evaluation of surface area and pore size distribution (IUPAC Technical Report), *Pure Appl. Chem.*, 2015, **87**(9–10), 1051–1069.

104 M. Schlichtenmayer and M. Hirscher, The usable capacity of porous materials for hydrogen storage, *Appl. Phys. A*, 2016, **122**(4), 379.

105 S. K. Bhatia and A. L. Myers, Optimum Conditions for Adsorptive Storage, *Langmuir*, 2006, **22**(4), 1688–1700.

106 D. E. Jaramillo, H. Z. H. Jiang, H. A. Evans, R. Chakraborty, H. Furukawa, C. M. Brown, *et al.*, Ambient-Temperature Hydrogen Storage via Vanadium(II)-Dihydrogen Complexation in a Metal–Organic Framework, *J. Am. Chem. Soc.*, 2021, **143**(16), 6248–6256.

107 M. P. Suh, H. J. Park, T. K. Prasad and D. W. Lim, Hydrogen Storage in Metal–Organic Frameworks, *Chem. Rev.*, 2012, **112**(2), 782–835.

108 K. M. Thomas, Hydrogen adsorption and storage on porous materials, *Catal. Today*, 2007, **120**(3), 389–398.
109 H. W. Langmi, J. Ren, B. North, M. Mathe and D. Bessarabov, Hydrogen Storage in Metal-Organic Frameworks: A Review, *Electrochim. Acta*, 2014, **128**, 368–392.
110 Y. S. Bae and R. Q. Snurr, Optimal isosteric heat of adsorption for hydrogen storage and delivery using metal–organic frameworks, *Microporous Mesoporous Mater.*, 2010, **132**(1), 300–303.
111 M. Schlichtenmayer and M. Hirscher, Nanosponges for hydrogen storage, *J. Mater. Chem.*, 2012, **22**(20), 10134–10143.
112 D. A. Gómez-Gualdrón, T. C. Wang, P. García-Holley, R. M. Sawelewa, E. Argueta, R. Q. Snurr, *et al.*, Understanding Volumetric and Gravimetric Hydrogen Adsorption Trade-off in Metal–Organic Frameworks, *ACS Appl. Mater. Interfaces*, 2017, **9**(39), 33419–33428.
113 Z. Chen, P. Li, R. Anderson, X. Wang, X. Zhang, L. Robison, *et al.*, Balancing volumetric and gravimetric uptake in highly porous materials for clean energy, *Science*, 2020, **368**(6488), 297–303.
114 D. Yuan, D. Zhao, D. Sun and H. C. Zhou, An Isoreticular Series of Metal–Organic Frameworks with Dendritic Hexacarboxylate Ligands and Exceptionally High Gas-Uptake Capacity, *Angew. Chem., Int. Ed.*, 2010, **49**(31), 5357–5361.
115 P. García-Holley, B. Schweitzer, T. Islamoglu, Y. Liu, L. Lin, S. Rodriguez, *et al.*, Benchmark Study of Hydrogen Storage in Metal–Organic Frameworks under Temperature and Pressure Swing Conditions, *ACS Energy Lett.*, 2018, **3**(3), 748–754.
116 A. Ahmed, S. Seth, J. Purewal, A. G. Wong-Foy, M. Veenstra, A. J. Matzger, *et al.*, Exceptional hydrogen storage achieved by screening nearly half a million metal-organic frameworks, *Nat. Commun.*, 2019, **10**(1), 1568.
117 P. Ramirez-Vidal, G. Sdanghi, A. Celzard and V. Fierro, High hydrogen release by cryo-adsorption and compression on porous materials, *Int. J. Hydrogen Energy*, 2022, **47**(14), 8892–8915.
118 W. Shi, X. Jin, C. Zhang, X. Zhang, X. Liu, Y. Gao, *et al.*, Recent advancement in metal-organic frameworks for hydrogen storage: Mechanisms, influencing factors and enhancement strategies, *Int. J. Hydrogen Energy*, 2024, **83**, 432–449.
119 X. Han, X. Yang, C. Yu, S. Lu, E. S. Pouya, P. Bai, *et al.*, Fine-tuning the pore structure of metal–organic frameworks by linker substitution for enhanced hydrogen storage and gas separation, *CrystEngComm*, 2021, **23**(16), 3026–3032.
120 R. M. Kumar, J. V. Sundar and V. Subramanian, Improving the hydrogen storage capacity of metal organic framework by chemical functionalization, *Int. J. Hydrogen Energy*, 2012, **37**(21), 16070–16077.
121 M. Dincă, A. F. Yu and J. R. Long, Microporous Metal–Organic Frameworks Incorporating 1,4-Benzeneditetrazolate: Syntheses, Structures, and Hydrogen Storage Properties, *J. Am. Chem. Soc.*, 2006, **128**(27), 8904–8913.
122 Z. Wang, K. K. Tanabe and S. M. Cohen, Tuning Hydrogen Sorption Properties of Metal–Organic Frameworks by Postsynthetic Covalent Modification, *Chem. – Eur. J.*, 2010, **16**(1), 212–217.
123 A. L. Sutton, J. I. Mardel and M. R. Hill, Metal-Organic Frameworks (MOFs) As Hydrogen Storage Materials At Near-Ambient Temperature, *Chem. – Eur. J.*, 2024, **30**(44), e202400717.
124 D. Sengupta, P. Melix, S. Bose, J. Duncan, X. Wang, M. R. Mian, *et al.*, Air-Stable Cu(I) Metal–Organic Framework for Hydrogen Storage, *J. Am. Chem. Soc.*, 2023, **145**(37), 20492–20502.
125 N. C. Burtch, H. Jasuja and K. S. Walton, Water Stability and Adsorption in Metal–Organic Frameworks, *Chem. Rev.*, 2014, **114**(20), 10575–10612.
126 S. Yuan, L. Feng, K. Wang, J. Pang, M. Bosch, C. Lollar, *et al.*, Stable Metal–Organic Frameworks: Design, Synthesis, and Applications, *Adv. Mater.*, 2018, **30**(37), 1704303.
127 J. A. Greathouse and M. D. Allendorf, The Interaction of Water with MOF-5 Simulated by Molecular Dynamics, *J. Am. Chem. Soc.*, 2006, **128**(33), 10678–10679.
128 G. G. Terrones, S. P. Huang, M. P. Rivera, S. Yue, A. Hernandez and H. J. Kulik, Metal–Organic Framework Stability in Water and Harsh Environments from Data-Driven Models Trained on the Diverse WS24 Data Set, *J. Am. Chem. Soc.*, 2024, **146**(29), 20333–20348.
129 P. Deria, D. A. Gómez-Gualdrón, W. Bury, H. T. Schaef, T. C. Wang, P. K. Thallapally, *et al.*, Ultraporous, Water Stable, and Breathing Zirconium-Based Metal–Organic Frameworks with ftw Topology, *J. Am. Chem. Soc.*, 2015, **137**(40), 13183–13190.
130 H. R. Fu, Z. X. Xu and J. Zhang, Water-Stable Metal–Organic Frameworks for Fast and High Dichromate Trapping via Single-Crystal-to-Single-Crystal Ion Exchange, *Chem. Mater.*, 2015, **27**(1), 205–210.
131 S. J. Yang, J. Y. Choi, H. K. Chae, J. H. Cho, K. S. Nahm and C. R. Park, Preparation and Enhanced Hydrostability and Hydrogen Storage Capacity of CNT@MOF-5 Hybrid Composite, *Chem. Mater.*, 2009, **21**(9), 1893–1897.
132 W. Zhang, Y. Hu, J. Ge, H. L. Jiang and S. H. Yu, A Facile and General Coating Approach to Moisture/Water-Resistant Metal–Organic Frameworks with Intact Porosity, *J. Am. Chem. Soc.*, 2014, **136**(49), 16978–16981.
133 X. Qian, R. Zhang, L. Chen, Y. Lei and A. Xu, Surface Hydrophobic Treatment of Water-Sensitive DUT-4 Metal–Organic Framework To Enhance Water Stability for Hydrogen Storage, *ACS Sustainable Chem. Eng.*, 2019, **7**(19), 16007–16012.
134 C. Schlemminger, E. Næss and U. Bünger, Adsorption hydrogen storage at cryogenic temperature – Material properties and hydrogen ortho-para conversion matters, *Int. J. Hydrogen Energy*, 2015, **40**(20), 6606–6625.
135 H. Wang, Z. Qu, W. Zhang and W. Tao, Effective Thermal Conductivity of MOF-5 Powder under a Hydrogen Atmosphere, *Computation*, 2015, **3**(4), 558–573.

136 L. Han, M. Budge and P. Alex Greaney, Relationship between thermal conductivity and framework architecture in MOF-5, *Comput. Mater. Sci.*, 2014, **94**, 292–297.
137 H. Babaei, A. J. H. McGaughey and C. E. Wilmer, Effect of pore size and shape on the thermal conductivity of metal-organic frameworks, *Chem. Sci.*, 2016, **8**(1), 583–589.
138 M. Islamov, H. Babaei, R. Anderson, K. B. Sezginel, J. R. Long, A. J. H. McGaughey, *et al.*, High-throughput screening of hypothetical metal-organic frameworks for thermal conductivity, *npj Comput. Mater.*, 2023, **9**(1), 1–12.
139 H. Babaei, M. E. DeCoster, M. Jeong, Z. M. Hassan, T. Islamoglu, H. Baumgart, *et al.*, Observation of reduced thermal conductivity in a metal-organic framework due to the presence of adsorbates, *Nat. Commun.*, 2020, **11**(1), 4010.
140 M. Islamov, H. Babaei and C. E. Wilmer, Influence of Missing Linker Defects on the Thermal Conductivity of Metal–Organic Framework HKUST-1, *ACS Appl. Mater. Interfaces*, 2020, **12**(50), 56172–56177.
141 B. Yeskendir, J. P. Dacquin, Y. Lorgouilloux, C. Courtois, S. Royer and J. Dhainaut, From metal–organic framework powders to shaped solids: recent developments and challenges, *Mater. Adv.*, 2021, **2**(22), 7139–7186.
142 G. T. Whiting, A. D. Chowdhury, R. Oord, P. Paalanen and B. M. Weckhuysen, The curious case of zeolite–clay/binder interactions and their consequences for catalyst preparation, *Faraday Discuss.*, 2016, **188**(0), 369–386.
143 J. Farrando-Pérez, M. Rodríguez-Castillo, M. Martínez-Escandell, M. Monge and J. Silvestre-Albero, Improved thermal management in HKUST-1 composites upon graphite flakes incorporation: Hydrogen adsorption properties, *Int. J. Hydrogen Energy*, 2023, **48**(93), 36474–36484.
144 R. Sule, A. K. Mishra and T. T. Nkambule, Recent advancement in consolidation of MOFs as absorbents for hydrogen storage, *Int. J. Energy Res.*, 2021, **45**(9), 12481–12499.
145 J. Łuczak, M. Kroczewska, M. Baluk, J. Sowik, P. Mazierski and A. Zaleska-Medynska, Morphology control through the synthesis of metal-organic frameworks, *Adv. Colloid Interface Sci.*, 2023, **314**, 102864.
146 K. Leng, Y. Sun, X. Li, S. Sun and W. Xu, Rapid Synthesis of Metal–Organic Frameworks MIL-101(Cr) Without the Addition of Solvent and Hydrofluoric Acid, *Cryst. Growth Des.*, 2016, **16**(3), 1168–1171.
147 G. Mouchaham, S. Wang and C. Serre, The Stability of Metal–Organic Frameworks, in *Metal–Organic Frameworks [Internet]*, ed. H. García and S. Navalón, Wiley, 1st edn, 2018, pp. 1–28. Available from: **https://onlinelibrary.wiley.com/doi/10.1002/9783527809097.ch1** [cited 2024 Feb 16].
148 H. U. Escobar-Hernandez, L. M. Pérez, P. Hu, F. A. Soto, M. I. Papadaki, H. C. Zhou, *et al.*, Thermal Stability of Metal–Organic Frameworks (MOFs): Concept, Determination, and Model Prediction Using Computational Chemistry and Machine Learning, *Ind. Eng. Chem. Res.*, 2022, **61**(17), 5853–5862.
149 S. A. Mohamed, S. Chong and J. Kim, Thermal Stability of Methyl-Functionalized MOF-5, *J. Phys. Chem. C*, 2019, **123**(49), 29686–29692.
150 M. Balcerzak, J. Ternieden and M. Felderhoff, Synthesis, thermal stability, and hydrogen storage properties of poorly crystalline TiVFeCuNb multi-principal element alloy: Dedicated to the memory of Michel Latroche and his great contribution to the field of metal hydrides, *J. Alloys Compd.*, 2023, **943**, 169142.
151 T. D. Bennett, T. K. Todorova, E. F. Baxter, D. G. Reid, C. Gervais, B. Bueken, *et al.*, Connecting defects and amorphization in UiO-66 and MIL-140 metal–organic frameworks: a combined experimental and computational study, *Phys. Chem. Chem. Phys.*, 2016, **18**(3), 2192–2201.
152 L. Valenzano, B. Civalleri, S. Chavan, S. Bordiga, M. H. Nilsen, S. Jakobsen, *et al.*, Disclosing the Complex Structure of UiO-66 Metal Organic Framework: A Synergic Combination of Experiment and Theory, *Chem. Mater.*, 2011, **23**(7), 1700–1718.
153 H. Tao, T. D. Bennett and Y. Yue, Melt-Quenched Hybrid Glasses from Metal–Organic Frameworks, *Adv. Mater.*, 2017, **29**(20), 1601705.
154 Y. N. Gong, D. C. Zhong and T. B. Lu, Interpenetrating metal–organic frameworks, *CrystEngComm*, 2016, **18**(15), 2596–2606.
155 F. D. Lahoz-Martín, S. Calero, J. J. Gutiérrez-Sevillano and A. Martin-Calvo, Adsorptive separation of ethane and ethylene using IsoReticular Metal-Organic Frameworks, *Microporous Mesoporous Mater.*, 2017, **248**, 40–45.
156 G. Verma, S. Butikofer, S. Kumar and S. Ma, Regulation of the Degree of Interpenetration in Metal–Organic Frameworks, *Top. Curr. Chem.*, 2020, **378**(1), 4.
157 L. Yuan, C. Zhang, Y. Zou, T. Bao, J. Wang, C. Tang, *et al.*, A S-Scheme MOF-on-MOF Heterostructure, *Adv. Funct. Mater.*, 2023, **33**(20), 2214627.
158 Z. Yu, J. Deschamps, L. Hamon, P. Karikkethu Prabhakaran and P. Pré, Hydrogen adsorption and kinetics in MIL-101(Cr) and hybrid activated carbon-MIL-101(Cr) materials, *Int. J. Hydrogen Energy*, 2017, **42**(12), 8021–8031.
159 P. B. Somayajulu Rallapalli, M. C. Raj, D. V. Patil, K. P. Prasanth, R. S. Somani and H. C. Bajaj, Activated carbon @ MIL-101(Cr): a potential metal-organic framework composite material for hydrogen storage, *Int. J. Energy Res.*, 2013, **37**(7), 746–753.
160 P. K. Prabhakaran and J. Deschamps, Room temperature hydrogen uptake in single walled carbon nanotubes incorporated MIL-101 doped with lithium: effect of lithium doping, *J. Porous Mater.*, 2015, **22**(6), 1635–1642.
161 J. G. Vitillo, L. Regli, S. Chavan, G. Ricchiardi, G. Spoto, P. D. C. Dietzel, *et al.*, Role of Exposed Metal Sites in Hydrogen Storage in MOFs, *J. Am. Chem. Soc.*, 2008, **130**(26), 8386–8396.
162 Y. E. Cheon and M. P. Suh, Enhanced Hydrogen Storage by Palladium Nanoparticles Fabricated in a Redox-Active Metal–Organic Framework, *Angew. Chem., Int. Ed.*, 2009, **48**(16), 2899–2903.
163 B. Szczęśniak, J. Choma and M. Jaroniec, Gas adsorption properties of hybrid graphene-MOF materials, *J. Colloid Interface Sci.*, 2018, **514**, 801–813.

164 X. Zhang, P. Liu and Y. Zhang, The application of MOFs for hydrogen storage, *Inorg. Chim. Acta*, 2023, **557**, 121683.
165 K. K. Gangu, S. Maddila, S. B. Mukkamala and S. B. Jonnalagadda, Characteristics of MOF, MWCNT and graphene containing materials for hydrogen storage: A review, *J. Energy Chem.*, 2019, **30**, 132–144.
166 M. C. Kreider, M. Sefa, J. A. Fedchak, J. Scherschligt, M. Bible, B. Natarajan, *et al.*, Toward 3D printed hydrogen storage materials made with ABS-MOF composites, *Polym. Adv. Technol.*, 2018, **29**(2), 867–873.
167 Z. Ma, J. Zou, D. Khan, W. Zhu, C. Hu, X. Zeng, *et al.*, Preparation and hydrogen storage properties of MgH_2-trimesic acid-TM MOF (TM=Co, Fe) composites, *J. Mater. Sci. Technol.*, 2019, **35**(10), 2132–2143.
168 D. H. Hong, H. S. Shim, J. Ha and H. R. Moon, MOF-on-MOF Architectures: Applications in Separation, Catalysis, and Sensing, *Bull. Korean Chem. Soc.*, 2021, **42**(7), 956–969.
169 J. Sánchez-Laínez, A. Veiga, B. Zornoza, S. R. G. Balestra, S. Hamad, A. R. Ruiz-Salvador, *et al.*, Tuning the separation properties of zeolitic imidazolate framework core–shell structures via post-synthetic modification, *J. Mater. Chem. A*, 2017, **5**(48), 25601–25608.
170 M. Ding, X. Cai and H. L. Jiang, Improving MOF stability: approaches and applications, *Chem. Sci.*, 2019, **10**(44), 10209–10230.
171 M. J. Manos, M. S. Markoulides, C. D. Malliakas, G. S. Papaefstathiou, N. Chronakis, M. G. Kanatzidis, *et al.*, A Highly Porous Interpenetrated Metal–Organic Framework from the Use of a Novel Nanosized Organic Linker, *Inorg. Chem.*, 2011, **50**(22), 11297–11299.
172 M. Gupta and J. J. Vittal, Control of interpenetration and structural transformations in the interpenetrated MOFs, *Coord. Chem. Rev.*, 2021, **435**, 213789.
173 H. L. Jiang, T. A. Makal and H. C. Zhou, Interpenetration control in metal–organic frameworks for functional applications, *Coord. Chem. Rev.*, 2013, **257**(15), 2232–2249.
174 F. G. Li, C. Liu, D. Yuan, F. Dai, R. Wang, Z. Wang, *et al.*, Ultrahigh Hydrogen Uptake in an Interpenetrated Zn_4O-Based Metal–Organic Framework, *CCS Chem.*, 2021, **4**(3), 832–837.
175 H. Jiang, Y. Feng, M. Chen and Y. Wang, Synthesis and hydrogen-storage performance of interpenetrated MOF-5/MWCNTs hybrid composite with high mesoporosity, *Int. J. Hydrogen Energy*, 2013, **38**(25), 10950–10955.
176 M. Xue, S. Ma, J. Z. Schaffino, R. M. Zhu, G. S. Lobkovsky, E. B, *et al.*, Robust Metal–Organic Framework Enforced by Triple-Framework Interpenetration Exhibiting High H_2 Storage Density, *Inorg. Chem.*, 2008, **47**(15), 6825–6828.
177 P. Kanoo, R. Matsuda, M. Higuchi, S. Kitagawa and T. K. Maji, New Interpenetrated Copper Coordination Polymer Frameworks having Porous Properties, *Chem. Mater.*, 2009, **21**(24), 5860–5866.
178 Y. Feng, H. Jiang, M. Chen and Y. Wang, Construction of an interpenetrated MOF-5 with high mesoporosity for hydrogen storage at low pressure, *Powder Technol.*, 2013, **249**, 38–42.
179 P.Á Szilágyi, M. Lutz, J. Gascon, J. Juan-Alcañiz, J. van Esch, F. Kapteijn, *et al.*, MOF@MOF core–shell vs. Janus particles and the effect of strain: potential for guest sorption, separation and sequestration, *CrystEngComm*, 2013, **15**(30), 6003–6008.
180 D. K. Panchariya, R. K. Rai, A. Kumar, E. Singh and S. K, Core–Shell Zeolitic Imidazolate Frameworks for Enhanced Hydrogen Storage, *ACS Omega*, 2018, **3**(1), 167–175.
181 P. Pachfule, Y. Chen, J. Jiang and R. Banerjee, Experimental and computational approach of understanding the gas adsorption in amino functionalized interpenetrated metal organic frameworks (MOFs), *J. Mater. Chem.*, 2011, **21**(44), 17737–17745.
182 D. J. Tranchemontagne, K. S. Park, H. Furukawa, J. Eckert, C. B. Knobler and O. M. Yaghi, Hydrogen Storage in New Metal–Organic Frameworks, *J. Phys. Chem. C*, 2012, **116**(24), 13143–13151.
183 B. Kesanli, Y. Cui, M. R. Smith, E. W. Bittner, B. C. Bockrath and W. Lin, Highly Interpenetrated Metal–Organic Frameworks for Hydrogen Storage, *Angew. Chem.*, 2005, **117**(1), 74–77.
184 V. Zeleňák and I. Saldan, Factors Affecting Hydrogen Adsorption in Metal–Organic Frameworks: A Short Review, *Nanomaterials*, 2021, **11**(7), 1638.
185 S. Ma, D. Sun, M. Ambrogio, J. A. Fillinger, S. Parkin and H. C. Zhou, Framework-Catenation Isomerism in Metal–Organic Frameworks and Its Impact on Hydrogen Uptake, *J. Am. Chem. Soc.*, 2007, **129**(7), 1858–1859.
186 L. Chai, J. Pan, Y. Hu, J. Qian and M. Hong, Rational Design and Growth of MOF-on-MOF Heterostructures, *Small*, 2021, **17**(36), 2100607.
187 Y. Gu, Y. N. Wu, L. Li, W. Chen, F. Li and S. Kitagawa, Controllable Modular Growth of Hierarchical MOF-on-MOF Architectures, *Angew. Chem.*, 2017, **129**(49), 15864–15868.
188 C. Liu, Q. Sun, L. Lin, J. Wang, C. Zhang, C. Xia, *et al.*, Ternary MOF-on-MOF heterostructures with controllable architectural and compositional complexity via multiple selective assembly, *Nat. Commun.*, 2020, **11**(1), 4971.
189 C. Liu, L. Lin, Q. Sun, J. Wang, R. Huang, W. Chen, *et al.*, Site-specific growth of MOF-on-MOF heterostructures with controllable nano-architectures: beyond the combination of MOF analogues, *Chem. Sci.*, 2020, **11**(14), 3680–3686.
190 P. Sanati-Tirgan, H. Eshghi and A. Mohammadinezhad, Designing a new method for growing metal–organic framework (MOF) on MOF: synthesis, characterization and catalytic applications, *Nanoscale*, 2023, **15**(10), 4917–4931.
191 K. Ikigaki, K. Okada, Y. Tokudome, T. Toyao, P. Falcaro, C. J. Doonan, *et al.*, MOF-on-MOF: Oriented Growth of Multiple Layered Thin Films of Metal–Organic Frameworks, *Angew. Chem., Int. Ed.*, 2019, **58**(21), 6886–6890.
192 T. Li, J. E. Sullivan and N. L. Rosi, Design and Preparation of a Core–Shell Metal–Organic Framework for Selective CO_2 Capture, *J. Am. Chem. Soc.*, 2013, **135**(27), 9984–9987.

193 C. Verma, T. Rasheed, M. T. Anwar and M. A. Quraishi, From metal-organic frameworks (MOFs) to metal-doped MOFs (MDMOFs): Current and future scenarios in environmental catalysis and remediation applications, *Microchem. J.*, 2023, **192**, 108954.

194 C. M. Wu, M. Rathi, S. P. Ahrenkiel, R. T. Koodali and Z. Wang, Facile synthesis of MOF-5 confined in SBA-15 hybrid material with enhanced hydrostability, *Chem. Commun.*, 2013, **49**(12), 1223–1225.

195 Z. Jaffar, N. M. Yunus, M. S. Shaharun, M. F. Allim and A. H. A. Rahim, Incorporated Metal–Organic Framework Hybrid Materials for Gas Separation, Catalysis and Wastewater Treatment, *Processes*, 2022, **10**(11), 2368.

196 J. D. Sosa, T. F. Bennett, K. J. Nelms, B. M. Liu, R. C. Tovar and Y. Liu, Metal–Organic Framework Hybrid Materials and Their Applications, *Crystals*, 2018, **8**(8), 325.

197 M. Muschi, S. Devautour-Vinot, D. Aureau, N. Heymans, S. Sene, R. Emmerich, *et al.*, Metal–organic framework/graphene oxide composites for CO_2 capture by microwave swing adsorption, *J. Mater. Chem. A*, 2021, **9**(22), 13135–13142.

198 A. Dutta, Y. Pan, J. Q. Liu and A. Kumar, Multicomponent isoreticular metal-organic frameworks: Principles, current status and challenges, *Coord. Chem. Rev.*, 2021, **445**, 214074.

199 M. Alfe, A. Policicchio, L. Lisi and V. Gargiulo, Solid sorbents for CO_2 and CH_4 adsorption: The effect of metal organic framework hybridization with graphene-like layers on the gas sorption capacities at high pressure, *Renewable Sustainable Energy Rev.*, 2021, **141**, 110816.

200 W. Zhang, Y. Liu, G. Lu, Y. Wang, S. Li, C. Cui, *et al.*, Mesoporous Metal–Organic Frameworks with Size-, Shape-, and Space-Distribution-Controlled Pore Structure, *Adv. Mater.*, 2015, **27**(18), 2923–2929.

201 L. He, Y. Liu, J. Liu, Y. Xiong, J. Zheng, Y. Liu, *et al.*, Core–Shell Noble-Metal@Metal-Organic-Framework Nanoparticles with Highly Selective Sensing Property, *Angew. Chem.*, 2013, **125**(13), 3829–3833.

202 H. Liu, L. Chang, C. Bai, L. Chen, R. Luque and Y. Li, Controllable Encapsulation of "Clean" Metal Clusters within MOFs through Kinetic Modulation: Towards Advanced Heterogeneous Nanocatalysts, *Angew. Chem.*, 2016, **128**(16), 5103–5107.

203 Z. Wang and S. M. Cohen, Postsynthetic modification of metal–organic frameworks, *Chem. Soc. Rev.*, 2009, **38**(5), 1315–1329.

204 P. K. Prabhakaran and J. Deschamps, Doping activated carbon incorporated composite MIL-101 using lithium: impact on hydrogen uptake, *J. Mater. Chem. A*, 2015, **3**(13), 7014–7021.

205 Z. Xiang, Z. Hu, W. Yang and D. Cao, Lithium doping on metal-organic frameworks for enhancing H_2 Storage, *Int. J. Hydrogen Energy*, 2012, **37**(1), 946–950.

206 C. Zlotea, R. Campesi, F. Cuevas, E. Leroy, P. Dibandjo, C. Volkringer, *et al.*, Pd Nanoparticles Embedded into a Metal-Organic Framework: Synthesis, Structural Characteristics, and Hydrogen Sorption Properties, *J. Am. Chem. Soc.*, 2010, **132**(9), 2991–2997.

207 S. J. Yang, J. H. Cho, K. S. Nahm and C. R. Park, Enhanced hydrogen storage capacity of Pt-loaded CNT@MOF-5 hybrid composites, *Int. J. Hydrogen Energy*, 2010, **35**(23), 13062–13067.

208 D. W. Lim, J. W. Yoon, K. Y. Ryu and M. P. Suh, Magnesium Nanocrystals Embedded in a Metal–Organic Framework: Hybrid Hydrogen Storage with Synergistic Effect on Physi- and Chemisorption, *Angew. Chem., Int. Ed.*, 2012, **51**(39), 9814–9817.

209 X. Hu, J. Wang, S. Li, X. Hu, R. Ye, L. Zhou, *et al.*, Pd-doped HKUST-1 MOFs for enhanced hydrogen storage: effect of hydrogen spillover, *RSC Adv.*, 2023, **13**(22), 14980–14990.

210 J. R. Varghese, C. Wendt, F. B. Dix, D. Aulakh, U. Sazama, A. A. Yakovenko, *et al.*, Design and Characterization of Metal Nanoparticle Infiltrated Mesoporous Metal–Organic Frameworks, *Inorg. Chem.*, 2021, **60**(17), 13000–13010.

211 S. N. Klyamkin, S. V. Chuvikov, N. V. Maletskaya, E. V. Kogan, V. P. Fedin, K. A. Kovalenko, *et al.*, High-pressure hydrogen storage on modified MIL-101 metal–organic framework, *Int. J. Energy Res.*, 2014, **38**(12), 1562–1570.

212 J. A. Villajos, G. Orcajo, G. Calleja, J. A. Botas and C. Martos, Beneficial cooperative effect between Pd nanoparticles and ZIF-8 material for hydrogen storage, *Int. J. Hydrogen Energy*, 2016, **41**(42), 19439–19446.

213 J. Jin, J. Ouyang and H. Yang, Pd Nanoparticles and MOFs Synergistically Hybridized Halloysite Nanotubes for Hydrogen Storage, *Nanoscale Res. Lett.*, 2017, **12**(1), 240.

214 N. M. Musyoka, J. Ren, H. W. Langmi, B. C. North, M. Mathe and D. Bessarabov, Synthesis of rGO/Zr-MOF composite for hydrogen storage application, *J. Alloys Compd.*, 2017, **724**, 450–455.

215 Z. Rao, K. Feng, B. Tang and P. Wu, Construction of well interconnected metal-organic framework structure for effectively promoting proton conductivity of proton exchange membrane, *J. Membr. Sci.*, 2017, **533**, 160–170.

216 Z. Chen, Z. G. Gu, W. Q. Fu, F. Wang and J. Zhang, A Confined Fabrication of Perovskite Quantum Dots in Oriented MOF Thin Film, *ACS Appl. Mater. Interfaces*, 2016, **8**(42), 28737–28742.

217 E. H. Otal, M. L. Kim, Y. Hattori, Y. Kitazawa, J. P. Hinestroza and M. Kimura, Versatile Covalent Postsynthetic Modification of Metal Organic Frameworks via Thermal Condensation for Fluoride Sensing in Waters, *Bioengineering*, 2021, **8**(12), 196.

218 K. P. Prasanth, P. Rallapalli, M. C. Raj, H. C. Bajaj and R. V. Jasra, Enhanced hydrogen sorption in single walled carbon nanotube incorporated MIL-101 composite metal–organic framework, *Int. J. Hydrogen Energy*, 2011, **36**(13), 7594–7601.

219 J. L. C. Rowsell and O. M. Yaghi, Strategies for Hydrogen Storage in Metal–Organic Frameworks, *Angew. Chem., Int. Ed.*, 2005, **44**(30), 4670–4679.

220 S. Liu, L. Sun, F. Xu, J. Zhang, C. Jiao, F. Li, *et al.*, Nanosized Cu-MOFs induced by graphene oxide and enhanced gas storage capacity, *Energy Environ. Sci.*, 2013, **6**, 818–823.

221 C. Petit, J. Burress and T. J. Bandosz, The synthesis and characterization of copper-based metal–organic framework/graphite oxide composites, *Carbon*, 2011, **49**(2), 563–572.

222 E. Rojas-Garcia, A. A. Castañeda-Ramírez, D. Angeles-Beltrán, R. López-Medina and A. M. Maubert-Franco, Enhancing in the hydrogen storage by SWCNT/HKUST-1 composites: Effect of SWCNT amount, *Catal. Today*, 2022, **394–396**, 357–364.

223 A. M. Varghese, K. S. K. Reddy and G. N. Karanikolos, An *In situ*-Grown Cu-BTC Metal–Organic Framework/Graphene Oxide Hybrid Adsorbent for Selective Hydrogen Storage at Ambient Temperature, *Ind. Eng. Chem. Res.*, 2022, **61**(18), 6200–6213.

224 S. Y. Lee and S. J. Park, Effect of platinum doping of activated carbon on hydrogen storage behaviors of metal-organic frameworks-5, *Int. J. Hydrogen Energy*, 2011, **36**(14), 8381–8387.

225 J. S. Li, Y. J. Tang, S. L. Li, S. R. Zhang, Z. H. Dai, L. Si, *et al.*, Carbon nanodots functional MOFs composites by a stepwise synthetic approach: enhanced H_2 storage and fluorescent sensing, *CrystEngComm*, 2015, **17**(5), 1080–1085.

226 K. Kamal, D. I. Grekov, A. M. Shariff, M. A. Bustam and P. Pré, Improving textural properties of magnesium-based metal-organic framework for gas adsorption by carbon doping, *Microporous Mesoporous Mater.*, 2021, **323**, 111246.

227 Y. Liu, P. Ghimire and M. Jaroniec, Copper benzene-1,3,5-tricarboxylate (Cu-BTC) metal-organic framework (MOF) and porous carbon composites as efficient carbon dioxide adsorbents, *J. Colloid Interface Sci.*, 2019, **535**, 122–132.

228 A. Domán, S. Klébert, J. Madarász, G. Sáfrán, Y. Wang and K. László, Graphene Oxide Protected Copper Benzene-1,3,5-Tricarboxylate for Clean Energy Gas Adsorption, *Nanomaterials*, 2020, **10**(6), 1182.

229 H. Zhu, K. Li, M. Chen, H. Cao and F. Wang, A Novel Metal–Organic Framework Route to Embed Co Nanoparticles into Multi-Walled Carbon Nanotubes for Effective Oxygen Reduction in Alkaline Media, *Catalysts*, 2017, **7**(12), 364.

230 J. Kim, S. Yeo, J. D. Jeon and S. Y. Kwak, Enhancement of hydrogen storage capacity and hydrostability of metal–organic frameworks (MOFs) with surface-loaded platinum nanoparticles and carbon black, *Microporous Mesoporous Mater.*, 2015, **202**, 8–15.

231 S. J. Yang and C. R. Park, Preparation of Highly Moisture-Resistant Black-Colored Metal Organic Frameworks, *Adv. Mater.*, 2012, **24**(29), 4010–4013.

232 K. Jayaramulu, K. K. R. Datta, C. Rösler, M. Petr, M. Otyepka, R. Zboril, *et al.*, Biomimetic Superhydrophobic/Superoleophilic Highly Fluorinated Graphene Oxide and ZIF-8 Composites for Oil-Water Separation, *Angew. Chem., Int. Ed.*, 2016, **55**(3), 1178–1182.

233 M. I. Nandasiri, J. Liu, B. P. McGrail, J. Jenks, H. T. Schaef, V. Shutthanandan, *et al.*, Increased Thermal Conductivity in Metal-Organic Heat Carrier Nanofluids, *Sci. Rep.*, 2016, **6**(1), 27805.

234 J. Purewal, D. Liu, A. Sudik, M. Veenstra, J. Yang, S. Maurer, *et al.*, Improved Hydrogen Storage and Thermal Conductivity in High-Density MOF-5 Composites, *J. Phys. Chem. C*, 2012, **116**(38), 20199–20212.

235 S. K. Gebremariam, L. F. Dumée, P. L. Llewellyn, Y. F. AlWahedi and G. N. Karanikolos, Metal-organic framework hybrid adsorbents for carbon capture – A review, *J. Environ. Chem. Eng.*, 2023, **11**(2), 109291.

236 G. Wang, E. Graham, S. Zheng, J. Zhu, R. Zhu, H. He, *et al.*, Diatomite-Metal-Organic Framework Composite with Hierarchical Pore Structures for Adsorption/Desorption of Hydrogen, Carbon Dioxide and Water Vapor, *Materials*, 2020, **13**(21), 4700.

237 H. S. Far, M. Najafi, M. Hasanzadeh and R. Rahimi, A 3D-printed hierarchical porous architecture of MOF@clay composite for rapid and highly efficient dye scavenging, *New J. Chem.*, 2022, **46**(48), 23351–23360.

238 F. Gao, Y. Li, Z. Bian, J. Hu and H. Liu, Dynamic hydrophobic hindrance effect of zeolite@zeolitic imidazolate framework composites for CO_2 capture in the presence of water, *J. Mater. Chem. A*, 2015, **3**(15), 8091–8097.

239 N. M. Musyoka, J. Ren, P. Annamalai, H. W. Langmi, B. C. North, M. Mathe, *et al.*, Synthesis of a hybrid MIL-101(Cr)/ZTC composite for hydrogen storage applications, *Res. Chem. Intermed.*, 2016, **42**(6), 5299–5307.